06/7/05

AF
JCW

Attorney Docket: NEX87/PCT-US
Express Mail Label No. EV: 730066897 US

IN THE UNITED STATES PATENT AND TRADEMARK OFFICE

APPLICANT:	PAGRATIS ET AL		
SERIAL NO.:	10/030,787	EXAMINER:	FORMAN, B.J.
FILED:	JANUARY 31, 2002	ART UNIT:	1634
TITLE:	HIGH AFFINITY TGFß NUCLEIC ACID LIGANDS AND INHIBITORS	CONFIRMATION NO.	6400

Mail Stop Appeal Brief
Commissioner for Patents
P.O. Box 1450
Alexandria, VA 22313-1450

SUPPLEMENT TO APPEAL BRIEF FILED ON May 31, 2005

Sir:

An Appeal Brief was filed in the referenced application on May 31, 2005. In the Evidence Appendix six references were cited as being enclosed; however these references were inadvertently not included with the brief. Enclosed with this Supplemental response are copies of the six references.

It is believed that no other fees are due with this Appeal Brief. If this is in error, please charge any additional fees to Deposit Account No. 19-5117.

Respectfully submitted,

Date: June 6, 2005

Rosemary Kellogg, #39,726
Swanson & Bratschun, L.L.C.
1745 Shea Center Drive, Suite 330
Highlands Ranch, Colorado 80129
Telephone: (303) 268-0066
Facsimile: (303) 268-0065

American Journal of Pathology, Vol. 154, No. 1, January 1999

Novel Approach to Specific Growth Factor Inhibition *in Vivo*

Antagonism of Platelet-Derived Growth Factor in Glomerulonephritis by Aptamers

Jürgen Floege,* Tammo Ostendorf,* Ulf Janssen,* Michael Burg,* Heinfried H. Radeke,† Chandra Vargeese,‡ Stanley C. Gill,‡ Louis S. Green,‡ and Nebojša Janjić‡

From the Divisions of Nephrology and Clinical Pharmacology,† Medizinische Hochschule, Hannover, Germany, and NeXstar Pharmaceuticals,‡ Boulder, Colorado*

Mesangial cell proliferation and matrix accumulation, driven by platelet-derived growth factor (PDGF), contribute to many progressive renal diseases. In a novel approach to antagonize PDGF, we investigated the effects of a nuclease-resistant high-affinity oligonucleotide aptamer *in vitro* and *in vivo*. In cultured mesangial cells, the aptamer markedly suppressed PDGF-BB but not epidermal- or fibroblast-growth-factor-2-induced proliferation. *In vivo* effects of the aptamer were evaluated in a rat mesangioproliferative glomerulonephritis model. Twice-daily intravenous (i.v.) injections from days 3 to 8 after disease induction of 2.2 mg/kg PDGF-B aptamer, coupled to 40-kd polyethylene glycol (PEG), led to 1) a reduction of glomerular mitoses by 64% on day 6 and by 78% on day 9, 2) a reduction of proliferating mesangial cells by 95% on day 9, 3) markedly reduced glomerular expression of endogenous PDGF B-chain, 4) reduced glomerular monocyte/macrophage influx on day 6 after disease induction, and 5) a marked reduction of glomerular extracellular matrix overproduction (as assessed by analysis of fibronectin and type IV collagen) both on the protein and mRNA level. The administration of equivalent amounts of a PEG-coupled aptamer with a scrambled sequence or PEG alone had no beneficial effect on the natural course of the disease. These data show that specific inhibition of growth factors using custom-designed, high-affinity aptamers is feasible and effective. *(Am J Pathol 1999, 154:169–179)*

Specific inhibition of growth factors and cytokines has become a major goal in experimental and clinical medicine. However, this approach is often hampered by the lack of specific pharmacological antagonists. Available alternative approaches are also limited, as neutralizing antibodies often show a low efficacy *in vivo* and may be immunogenic, and as *in vivo* gene therapy for these purposes is still in its infancy. In the present study we have investigated a novel approach to specifically inhibit growth factors *in vivo*, namely, the use of aptamers produced by the systematic evolution of ligands by exponential enrichment (SELEX) method.[1,2] The SELEX method has recently emerged as a powerful tool for screening large sequence-randomized nucleic acid libraries for unique oligonucleotides (aptamers) that bind to various other molecules with high affinity and specificity. For the purpose of this study, we have targeted platelet-derived growth factor (PDGF), the role of which is particularly well established in cardiovascular and renal disease.[3,4]

A large variety of progressive renal diseases is characterized by glomerular mesangial cell proliferation and matrix accumulation.[5] PDGF B-chain appears to have a central role in driving both of these processes given that 1) mesangial cells produce PDGF *in vitro* and various growth factors induce mesangial cell proliferation via induction of auto- or paracrine PDGF B-chain excretion, 2) PDGF B-chain and its receptor are overexpressed in many glomerular diseases, 3) infusion of PDGF-BB or glomerular transfection with a PDGF B-chain cDNA can induce selective mesangial cell proliferation and matrix accumulation *in vivo*, and 4) PDGF B-chain or β-receptor knock-out mice fail to develop a mesangium (reviewed in Ref. 4).

So far only one study has examined the effect of inhibition of PDGF B-chain in renal disease; Johnson et al,

Supported by a grant (SFB 244/C12) and a Heisenberg stipend of the Deutsche Forschungsgemeinschaft to J. Floege.

Accepted for publication October 11, 1998.

J. Floege and T. Ostendorf contributed equally to this study.

Address reprint requests to Dr. Jürgen Floege, Division of Nephrology 6840, Medizinische Hochschule, 30623 Hannover, Germany (E-mail: Floege.Juergen@MH-Hannover.de) or Nebojsa Janjic, Ph.D., NeXstar Pharmaceuticals, Inc., 2860 Wilderness Place, Boulder, CO 80301; E-mail: njanjic@nexstar.com.

using a neutralizing polyclonal antibody to PDGF, were able to reduce mesangial cell proliferation and matrix accumulation in a rat model of mesangioproliferative glomerulonephritis.[6] In this model, injection of an anti-mesangial cell antibody (anti-Thy-1.1) results in complement-dependent lysis of the mesangial cells, followed by an overshooting reparative phase that resembles human mesangioproliferative nephritis.[7] Limitations of the study of Johnson et al[6] included the necessity to administer large amounts of heterologous IgG and a limitation of the study duration to 4 days due to concerns that the heterologous IgG might elicit a humoral immune reaction. In the present study we have therefore used the anti-Thy-1.1 nephritis model to evaluate the feasibility and efficacy of inhibiting PDGF B-chain *in vivo* with high-affinity DNA-based aptamers.

Materials and Methods

Synthesis of High-Affinity DNA-Based Aptamers to the PDGF B-Chain

All aptamers and their sequence-scrambled controls were synthesized by the solid-phase phosphoramidite method on controlled pore glass using an 8800 Milligen DNA synthesizer and deprotected using ammonium hydroxide at 55°C for 16 hours. 2-Fluoropyrimidine nucleoside phosphoramidites were obtained from JBL Scientific (San Luis Obispo, CA). 2′-*O*-Methylpurine phosphoramidites were obtained from PerSeptive Biosystems (Boston, MA). Hexaethylene glycol (18-atom) spacer was obtained from Glen Research (Sterling, VA). All other nucleoside phosphoramidites were from PerSeptive Biosystems. To prolong the *in vivo* half-time of the aptamers in plasma, they were coupled to 40-kd polyethylene glycol (PEG). The covalent coupling of PEG to the aptamer (or to its sequence-scrambled control) was accomplished by treating 40-kd PEG *N*-hydroxysuccinimide ester (Shearwater Polymers, Huntsville, AL) with a primary amine group introduced at the 5′ end of the aptamer using trifluoroacetyl-protected pentylamine phosphoramidite. All PEG-aptamer conjugates were purified by anion exchange followed by reverse-phase high-pressure liquid chromatography (HPLC). The binding affinities of various aptamers for PDGF-AB or -BB (R&D Systems, Minneapolis, MN) were determined by the nitrocellulose filter binding method[8] or by the competition electrophoresis mobility shift assay.[9]

Cloning and Expression of Rat PDGF-BB

Rat PDGF-BB for cross-reactivity binding experiments was derived from *Escherichia coli* transfected with sCR-Script Amp SK(+) plasmid containing the rat PDGF-BB sequence. Rat PDGF-BB sequence was derived from rat lung poly A+ RNA (Clontech, San Diego, CA) through reverse transcription polymerase chain reaction (RT-PCR) using primers that amplify sequence encoding the mature form of PDGF-BB. Rat PDGF-BB protein expression and purification was performed at R&D Systems.

Stability of Aptamers in Rat Plasma in Vitro *and* in Vivo

The stabilities of DNA-based aptamers *in vitro* were examined in rat serum at 37°C. Serum was obtained from a Sprague-Dawley rat and was filtered through a 0.45-μm cellulose acetate filter and buffered with 20 mmol/L sodium phosphate buffer. Test ligands were added to the serum at the final concentration of 500 nmol/L. The final serum concentration was 85% as a result of the addition of buffer and aptamer. From the original 900-μl incubation mixture, 100-μl aliquots were withdrawn at various time points and added to 10 μl of 500 mmol/L EDTA (pH 8.0), mixed and frozen on dry ice, and stored at −20°C until the end of the experiment. The amount of full-length oligonucleotide ligand remaining at each of the time points was quantitated by HPLC analysis. To prepare the samples for HPLC injections, 200 μl of a mixture of 30% formamide, 70% 25 mmol/L Tris buffer (pH 8.0) containing 1% acetonitrile was added to 100 μl of thawed time point samples, mixed for 5 seconds, and spun for 20 minutes at 14,000 rpm in an Eppendorf microcentrifuge. The analysis was performed using an anion exchange chromatography column (NuceoPac, Dionex, PA-100, 4 × 50 mm) applying a LiCl gradient. The amount of full-length oligonucleotide remaining at each time point was determined from the peak areas.

Pharmacokinetics of the Modified PDGF Aptamer Conjugated to 40-kd PEG in Vivo

The pharmacokinetic properties of the modified PDGF aptamer conjugated to 40-kd PEG were determined in Sprague-Dawley rats. Before animal dosing, the aptamer was diluted with sterile PBS from a stock solution (also in sterile PBS), to final concentrations between 1 and 2 mg/ml (based on oligonucleotide molecular weight and the ultraviolet absorption at 260 nm with an extinction coefficient of 0.037 per mg oligo/ml). A single dose of the aptamer was administered to three Sprague-Dawley rats by i.v. bolus injection through the tail vein. Blood samples (approximately 400 μl) were obtained by venipuncture under isofluorane anesthesia and placed in EDTA-containing tubes. The EDTA blood samples were immediately processed by centrifugation to attain plasma and stored frozen at ≤−20°C. Time points for blood sample collection ranged from 2 to 480 minutes

To prepare plasma samples for HPLC analysis, 200 μl of methanol was added to 100 μl of plasma sample, mixed for 30 seconds, and spun in a centrifuge for 10 minutes at 15,000 × *g*. All of the supernatant was transferred to a new tube and dried under vacuum. Samples were resuspended by addition of 100 μl of 50% formamide and 4% perchloric acid, mixed, and spun as described above. Ninety microliters of supernatant was transferred to a 250-μl limited-volume insert vial for HPLC analysis. Samples were analyzed by anion exchange HPLC (DNAPac PA-100, 4 × 50 mm) with LiCl gradient elution in 30% formamide and monitoring of ultraviolet absorption at 270 nm. Aptamer concentrations were de-

termined based on peak area from a standard curve of the PEG-aptamer conjugate. The HPLC-based analysis described here and the double hybridization analysis described previously[9] have produced comparable results for a similar aptamer conjugated to 40-kd PEG (specific binding to vascular endothelial growth factor, Stanley C. Gill, unpublished observations), suggesting that the HPLC analysis indicates the levels of undegraded (full-length) aptamer. Nevertheless, as the PEG moiety has a strong influence on the HPLC retention times of the PEG-aptamer conjugate, we have not at this time ruled out the possibility that some of the partially degraded aptamer may migrate with a similar retention time as the full-length aptamer.

Mesangial Cell Culture Experiments

Human and rat mesangial cells were established in culture, characterized, and maintained as described previously.[10] To examine the antiproliferative effect of the aptamers on the cultured mesangial cells, cells were seeded in 96-well plates (Nunc, Wiesbaden, Germany) and grown to subconfluency. They were then growth-arrested for 48 hours in MCDB 302 medium (Sigma, Deisenhofen, Germany) (human mesangial cells) or RPMI 1640 with 1% bovine serum albumin (rat mesangial cells). After 48 hours, various stimuli together with PDGF B-chain aptamer or sequence-scrambled aptamer were added: medium alone, human recombinant PDGF-AA, -AB, or -BB (kindly provided by J. Hoppe, University of Würzburg, Germany), human recombinant epidermal growth factor (EGF; Calbiochem, Bad Soden, Germany), or recombinant human fibroblast growth factor-2 (kindly provided by Synergen/Amgen, Boulder, CO). DNA synthesis in the rat mesangial cells was determined by [^{3}H]thymidine incorporation as described[11] after 24 hours of stimulation (of which the last 4 hours were in the presence of [^{3}H]thymidine). In the case of human mesangial cells, after 72 hours of incubation, numbers of viable cells were determined using 2,3-bis[2-methoxy-4-nitro-5-sulfophenyl]-2H-tetrazolium-5-carboxanilide (XTT; Sigma) as described.[12]

Experimental Design

All animal experiments were approved by the local review boards. Anti-Thy-1.1 mesangial proliferative glomerulonephritis was induced in 33 male Wistar rats (Charles River, Sulzfeld, Germany) weighing 150 to 160 g by injection of 1 mg/kg monoclonal anti-Thy-1.1 antibody (clone OX-7; European Collection of Animal Cell Cultures, Salisbury, UK). Rats were treated with aptamers or PEG (see below) from days 3 to 8 after disease induction. Treatment consisted of twice-daily i.v. bolus injections of the substances dissolved in 400 μl of PBS, pH 7.4, for a total of 12 injections. The treatment duration was chosen to treat rats from ~1 day after the onset to the peak of mesangial cell proliferation, which in the OX-7-induced anti-Thy-1.1 nephritis occurs between days 6 and 9 after disease induction. Four groups of rats were studied: 1) 9 rats that received a total of 4 mg (0.33 mg/injection) of the PDGF-B aptamer (coupled to 15.7 mg 40 kd PEG), 2) 10 rats that received an equivalent amount of PEG-coupled, scrambled aptamer, 3) 8 rats that received an equivalent amount (15.7 mg) of 40-kd PEG alone, and 4) 6 rats that received 400-μl bolus injections of PBS alone. Renal biopsies for histological evaluation were obtained on day 6 by intravital biopsy and postmortem on day 9 after disease induction. For intravital biopsies the left kidney was exposed by a flank incision under general anesthesia. A 3- to 4-mm slice was then cut off the lower pole, and bleeding was stopped immediately by gently applying a collagen sponge, followed by wound closure. As judged from serum creatinines, this biopsy technique does not disturb renal function (unpublished observations). Twenty-four-hour urine collections were performed from days 5 to 6 and 8 to 9 after disease induction. The thymidine analogue 5-bromo-2'-deoxyuridine (BrdU; Sigma; 100 mg/kg body weight) was injected intraperitoneally at 4 hours before sacrifice on day 9.

Normal ranges of proteinuria and renal histological parameters (see below) were established in 10 nonmanipulated Wistar rats of similar age.

Renal Morphology

Tissue for light microscopy and immunoperoxidase staining was fixed in methyl Carnoy's solution[13] and embedded in paraffin. Four-micron sections were stained with the periodic acid Schiff (PAS) reagent and counterstained with hematoxylin. In the PAS-stained sections the number of mitoses within 100 glomerular tufts was determined.

Immunoperoxidase Staining

Four-micron sections of methyl Carnoy's-fixed biopsy tissue were processed by an indirect immunoperoxidase technique as described.[13] Primary antibodies were identical to those described previously[14,15] and included a murine monoclonal antibody (clone 1A4) to α-smooth muscle actin; a murine monoclonal antibody (clone PGF-007) to PDGF B-chain; a murine monoclonal IgG antibody (clone ED1) to a cytoplasmic antigen present in monocytes, macrophages, and dendritic cells; affinity-purified polyclonal goat anti-human/bovine type IV collagen IgG preabsorbed with rat erythrocytes; an affinity-purified IgG fraction of a polyclonal rabbit anti-rat fibronectin antibody; plus appropriate negative controls as described previously.[14,15] Evaluation of all slides was performed by an observer who was unaware of the origin of the slides.

To obtain mean numbers of infiltrating leukocytes in glomeruli, more than 50 consecutive cross sections of glomeruli were evaluated and mean values per kidney were calculated. For the evaluation of the immunoperoxidase stains for α-smooth muscle actin and PDGF B-chain, each glomerular area was graded semiquantitatively, and the mean score per biopsy was calculated. Each score reflects mainly changes in the extent rather than intensity of staining and depends on the percentage

of the glomerular tuft area showing focally enhanced positive staining: I, 0% to 25%; II, 25% to 50%; III, 50% to 75%; IV, >75%. We have recently described that data obtained using this scoring system are highly correlated with those obtained by computerized morphometry.[16,17]

Immunohistochemical Double Staining

Double immunostaining for the identification of the type of proliferating cells was performed as reported previously[16,17] by first staining the sections for proliferating cells with a murine monoclonal antibody (clone BU-1) against bromodeoxyuridine-containing nuclease in Tris-buffered saline (Amersham, Braunschweig, Germany) using an indirect immunoperoxidase procedure. Sections were then incubated with the IgG_1 monoclonal antibodies 1A4 against α-smooth muscle actin and ED1 against monocytes/macrophages. Cells were identified as proliferating mesangial cells or monocytes/macrophages if they showed positive nuclear staining for BrdU and if the nucleus was completely surrounded by cytoplasm positive for α-smooth muscle actin or ED1 antigen. Negative controls included omission of either of the primary antibodies, in which case no double staining was noted.

In Situ *Hybridization for Type IV Collagen mRNA*

In situ hybridization was performed on 4-μm sections of biopsy tissue fixed in buffered 10% formalin using a digoxigenin-labeled antisense RNA probe for type IV collagen[18] as described.[14] Detection of the RNA probe was performed with an alkaline-phosphatase-coupled anti-digoxigenin antibody (Genius nonradioactive nucleic acid detection kit, Boehringer-Mannheim, Mannheim, Germany) with subsequent color development. Controls consisted of hybridization with a sense probe to matched serial sections by hybridization of the antisense probe to tissue sections that had been incubated with RNAse A before hybridization or by deletion of the probe, antibody, or color solution.[15] Glomerular mRNA expression was semiquantitatively assessed using the scoring system described above.

Miscellaneous Measurements

Urinary protein was measured using the Bio-Rad protein assay (Bio-Rad Laboratories, München, Germany) and bovine serum albumin (Sigma) as a standard.

Statistical Analysis

All values are expressed as means ± SD. Statistical significance (defined as $P < 0.05$) was evaluated using Student *t*-tests or analysis of variance and Bonferroni *t*-tests.

Results

Post-SELEX Modifications in PDGF DNA Aptamers Result in Improved Nuclease Resistance

High-affinity DNA aptamers to the PDGF B-chain were identified previously by the SELEX process.[8] The consensus secondary structure motif of these aptamers is a three-way helix junction with a conserved single-stranded loop at the point of strand exchange (Figure 1A). To improve nuclease resistance of one of the minimal aptamers (a truncated version of aptamer 36t in Ref. 8), we have synthesized and tested a series of 2′-*O*-methyl- or 2′-fluoro-substituted aptamers to identify positions that tolerate such substitutions without a loss of binding affinity. In addition to identifying a pattern of allowed 2′-*O*-methyl- and 2′-fluoro substitutions, we found that trinucleotide loops on helices II and III in the aptamer could be replaced with hexaethylene glycol (18-atom) non-nucleotide spacers without compromising high-affinity binding to PDGF-AB or -BB (Figure 1A). This finding is in agreement with the notion that the helix junction domain of the aptamer represents the core of the structural motif required for high-affinity binding.[8] In practical terms, the replacement of six nucleotides with two spacers is advantageous in that it reduces by four the number of coupling steps required for the synthesis of the aptamer. Another support for the importance of helix junction domain in binding comes from the control aptamer, in which eight nucleotides in the helix junction region were interchanged without formally changing the consensus secondary structure (Figure 1A). The binding affinity of this scrambled aptamer for PDGF-BB ($K_d \approx 1$ μmol/L) is 10,000-fold lower compared with the binding affinity of the aptamer used in the experiments described below ($K_d \approx 0.1$ nmol/L).

We next compared the stabilities of the modified aptamer and its precursor DNA aptamer in rat serum *in vitro*. The half-time of the modified aptamer in serum was considerably longer (~8 hours) compared with that of its all-DNA precursor (~0.6 hours; Figure 1B). The observed increase in nuclease resistance is in agreement with previous studies with 2′-substituted nucleic acids.[19,20] In addition to the modifications mentioned above, for all experiments reported here, the modified DNA aptamer was conjugated to 40-kd PEG. Importantly, the addition of the PEG moiety to the 5′ end of the aptamer has no effect on the binding affinity of the aptamer for PDGF-BB ($K_d \approx 0.1$ nmol/L).

Pharmacokinetics of the Modified PDGF Aptamer Conjugated to 40-kd PEG in Vivo

The concentration of the modified PDGF aptamer conjugated to 40-kd PEG in rat plasma after i.v. injection (1 mg/kg) is shown in Figure 1C. The clearance of the aptamer-PEG conjugate from plasma is biphasic with approximately 47% of the compound being cleared with a half-life of 32.4 ± 13 minutes and 53% of the compound

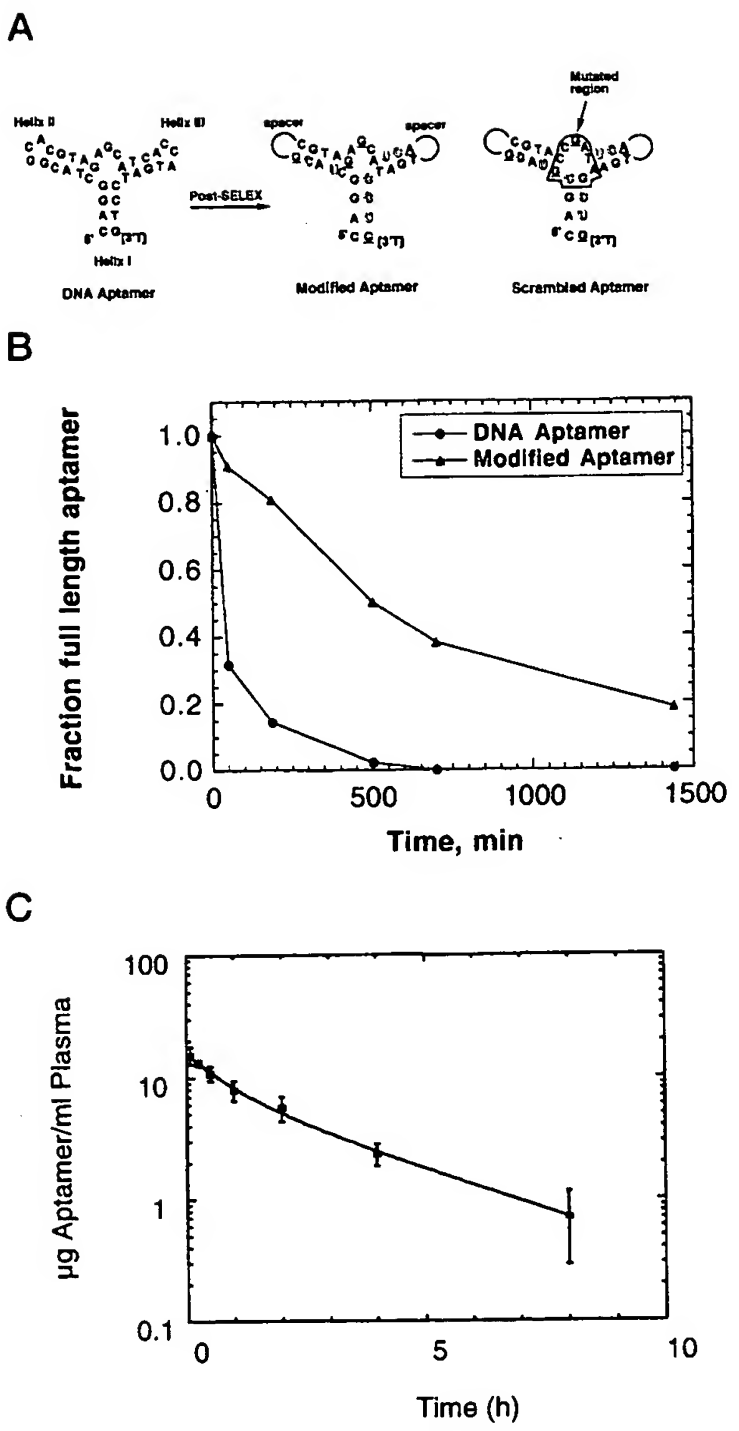

Figure 1. A: Summary of post-SELEX modifications in the PDGF B-chain aptamers. Outlined and underlined letters denote 2′-fluoro and 2′-*O*-methyl nucleotides, respectively; spacer indicates the hexaethylene glycol linker, and [3′T] indicates an inverted (3′-3′) thymidine nucleotide used as a cap to reduce 3′ to 5′ exonuclease-mediated digestion. The mutated region of the scrambled region is boxed to accent the overall similarity to the aptamer. B: Stability of the all-DNA aptamer and the modified PDGF B-chain aptamers in rat serum at 37°C *in vitro*. C: Plasma concentration of modified PDGF-B aptamer conjugated to 40-kd PEG in Sprague-Dawley rats (mean ± SD; n = 3). Compartmental pharmacokinetic analysis (curve fit) was carried out using WinNonlin, version 1.5 (Scientific Consulting Apex, NC).

being cleared with a half-life of 134.5 ± 13 minutes. The concentration of the aptamer in rat plasma after the i.v. injection is 16 µg/ml (1.6 µmol/L) at t = 0 and 0.21 µg/ml (21 nmol/L) at t = 12 hours (extrapolated). Thus, to a first approximation and assuming a linear increase in plasma concentration of the aptamer at the higher injected dose in the experiments described below (2.1 to 2.2 mg/kg i.v. every 12 hours), the aptamer concentration during the treatment period was not lower than 40 nmol/L (ie, 0.4 µg/ml).

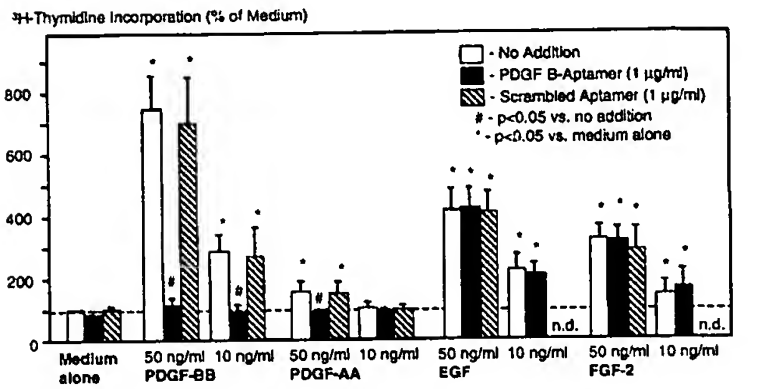

Figure 2. Effects of PDGF-B aptamer on mitogen-stimulated DNA synthesis of rat mesangial cells in culture. Data are 4-hour [^{3}H]thymidine incorporation rates and are expressed as percentage of baseline incorporation (medium alone with no addition, 1373 ± 275 cpm). Data are means ± SD of five independent experiments.

Cross-Reactivity of Aptamers for Rat PDGF-BB

The sequence of PDGF is highly conserved among species, and human and rat PDGF B-chain sequences are 89% identical.[21,22] Nevertheless, in view of the high specificity of aptamers,[23] the correct interpretation of the *in vivo* experiments requires understanding of the binding properties of the aptamers to rat PDGF B-chain. We have therefore cloned and expressed the mature form of rat PDGF-BB in *E. coli*. Based on nitrocellulose filter binding experiments, the PDGF aptamers bound to rat and human recombinant PDGF-BB with the same affinity ($K_d \approx$ 0.1 nmol/L).

PDGF B-Chain DNA-Aptamer Specifically Inhibits PDGF-BB-Induced Rat and Human Mesangial Cell Proliferation in Vitro

In growth-arrested rat mesangial cells, the effects of the PDGF-B aptamer or the scrambled aptamer on mitogen-induced proliferation were tested. Stimulated growth rates of the cells were not affected by the addition of scrambled aptamer (Figure 2). At a concentration of 1 µg/ml the PDGF-B aptamer completely inhibited the PDGF-BB- and -AA-induced growth but had no effect on EGF- or FGF-2-induced growth (Figure 2). In an additional experiment we also documented a 84% inhibition of the mesangial cell growth induced by 50 ng/ml PDGF-BB at an aptamer concentration of 0.5 µg/ml, ie, the minimal aptamer level achieved *in vivo* (see above). Inhibition of PDGF-BB-induced growth by the PDGF-B aptamer was not due to cell death as evidenced by trypan blue exclusion of the cells. Furthermore, using morphological criteria, in particular, nuclear condensation, no evidence for mesangial cell apoptosis was noted under these conditions.

Using the XTT assay (Table 1), the PDGF-B aptamer also completely inhibited PDGF-BB-induced human mesangial cell growth. PDGF-AB- and -AA-induced mesangial cell growth also tended to be lower with the PDGF-B aptamer, but these differences failed to reach statistical significance. In contrast, no effects of the PDGF-B aptamer on either EGF- or FGF-2-induced growth were noted (Table 1). Similar effects were noted if the aptam-

Table 1. Effects of PDGF-B Aptamer on Mitogen-Stimulated Proliferation of Human Mesangial Cells in Culture

	Medium	PDGF-BB	PDGF-AB	PDGF-AA	EGF	FGF-2
PDGF-B aptamer (50 μg/ml)	98 ± 23	108 ± 15*	76 ± 34	100 ± 29	159 ± 14	162 ± 20
Scrambled aptamer (50 μg/ml)	88 ± 19	228 ± 65	123 ± 36	142 ± 41	160 ± 21	163 ± 38
40-kd PEG alone	100 ± 0	218 ± 92	159 ± 40	142 ± 56	155 ± 33	174 ± 22

All mitogens were added at 100 ng/ml final concentration. Data are optical densities measured in the XTT assay and are expressed as percentages of baseline, ie, cells stimulated with medium plus 200 μg/ml 40-kd PEG (ie, the amount equivalent to the PEG attached to 50 μg/ml aptamer). Results are means ± SD of five separate experiments (n = 3 in the case of medium plus 40-kd PEG; statistical evaluation was therefore confined to the PDGF-B and scrambled aptamer groups.

*$P < 0.05$ *versus* scrambled aptamer.

ers were used at a concentration of 10 μg/ml (data not shown).

Effects of PDGF B-Chain DNA-Aptamer in Rats with Anti-Thy-1.1 Nephritis

After the injection of anti-Thy-1.1 antibody, PBS-treated animals developed the typical course of the nephritis, which is characterized by early mesangiolysis and followed by a phase of mesangial cell proliferation and matrix accumulation on days 6 and 9. No obvious adverse effects were noted after the repeated injection of aptamers or PEG alone, and all rats survived and appeared normal until the end of the study.

In PAS-stained renal sections the mesangioproliferative changes on days 6 and 9 after disease induction were severe and indistinguishable among rats receiving PBS, PEG alone, or the scrambled aptamer (Figure 3, A to C). Histological changes were markedly reduced in the PDGF-B aptamer-treated group (Figure 3D). To evaluate the mesangioproliferative changes, various parameters were analyzed.

Reduction of Mesangial Cell Proliferation

Glomerular cell proliferation, as assessed by counting the number of glomerular mitoses, was not significantly different between the three control groups on days 6 and 9 (Figure 4). Compared with rats receiving the scrambled aptamer, treatment with PDGF-B aptamer led to a reduction of glomerular mitoses by 64% on day 6 and by 78% on day 9 (Figure 4). To assess the treatment

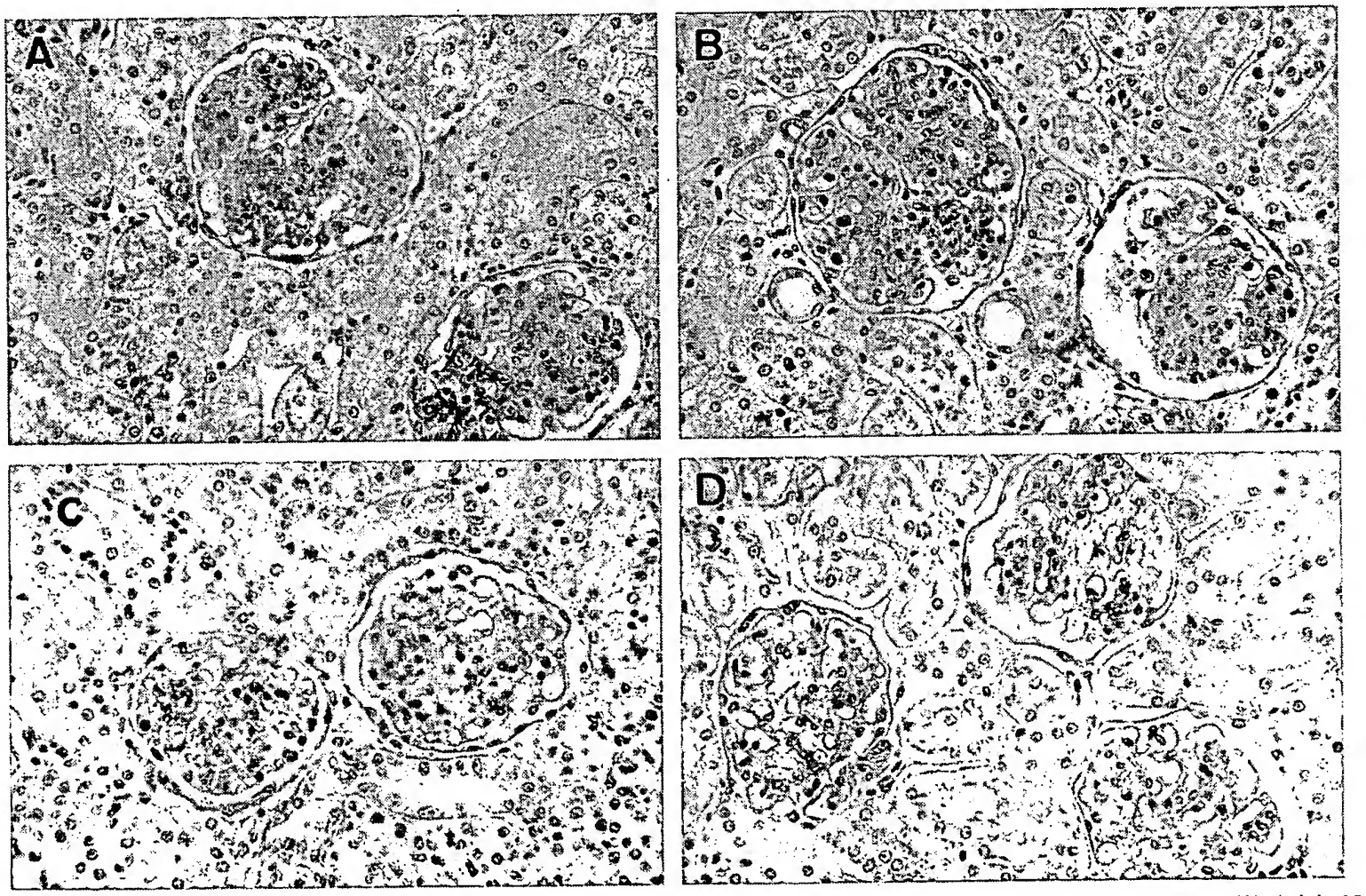

Figure 3. Representative PAS-stained renal sections at day 9 after disease induction of mesangioproliferative nephritis of a rat receiving PBS alone (A), 40-kd PEG alone (B), scrambled aptamer coupled to 40-kd PEG (C), or PDGF-B aptamer coupled to 40-kd PEG (D). Compared with the three control rats shown in A to C, the PDGF-B aptamer-treated rat exhibits an almost normal glomerular morphology, ie, markedly reduced glomerular hypercellularity and mesangial matrix accumulation. Magnification, ×400.

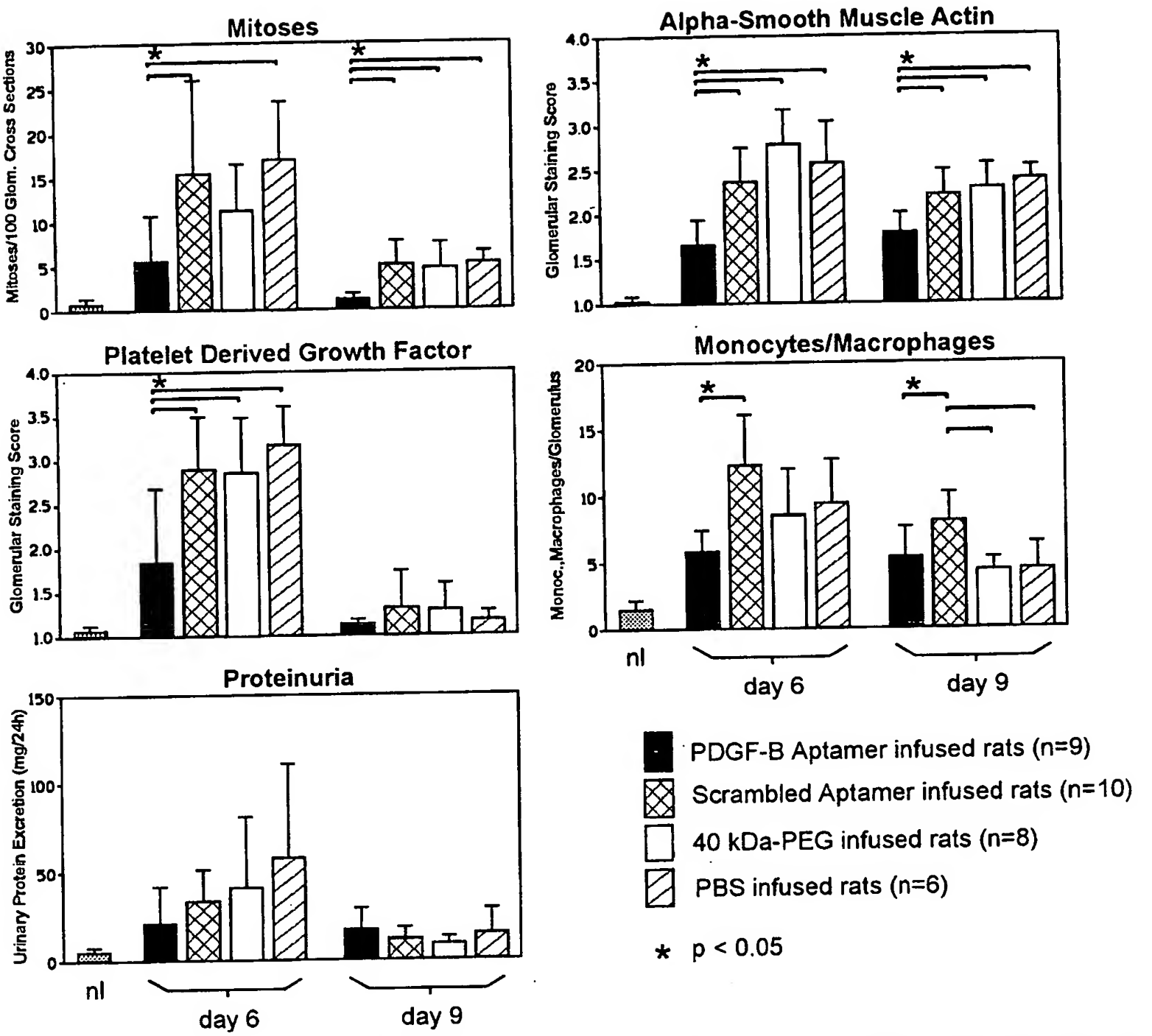

Figure 4. Effects of PDGF-B aptamer on glomerular cell proliferation, mesangial cell activation (as assessed by glomerular *de novo* expression of α-smooth muscle actin), expression of glomerular PDGF B-chain, monocyte/macrophage influx, and proteinuria in rats with anti-Thy-1.1 nephritis. nl = values observed in 10 normal rats.

effects on mesangial cells, we immunostained the renal sections for α-smooth muscle actin, which is expressed by activated mesangial cells only.[24] Again, there were no significant differences between the three control groups on days 6 and 9. However, the immunostaining scores of α-smooth muscle actin were significantly reduced on days 6 and 9 in the PDGF-B aptamer-treated group (Figure 4). To specifically determine whether mesangial cell proliferation was reduced, we double immunostained PDGF-B aptamer-treated rats and scrambled aptamer-treated rats for a cell proliferation marker (BrdU) and α-smooth muscle actin. The data confirmed a marked decrease of proliferating mesangial cells on day 9 after disease induction: 2.2 ± 0.8 BrdU-positive/α-smooth-muscle-actin-positive cells per 100 glomerular cross sections in PDGF-B aptamer-treated rats *versus* 43.3 ± 12.4 cells in rats receiving the scrambled aptamer, ie, a 95% reduction of mesangial cell proliferation (Figure 5). In contrast, no effect of the PDGF-B aptamer was noted on proliferating monocytes/macrophages on day 9 after disease induction (PDGF-B aptamer-treated rats: 2.8 ± 1.1 $BrdU^+/ED\text{-}1^+$ cells per 100 glomerular cross sections; scrambled aptamer-treated rats: 2.7 ± 1.8).

Reduced Expression of Endogenous PDGF B-Chain

By immunohistochemistry the glomerular PDGF B-chain expression was markedly up-regulated in all three control groups (Figure 4), similar to previous observations.[15] In the PDGF-B aptamer-treated group the glomerular overexpression of PDGF B-chain was significantly reduced in parallel with the reduction of proliferating mesangial cells (Figure 4). This reduction

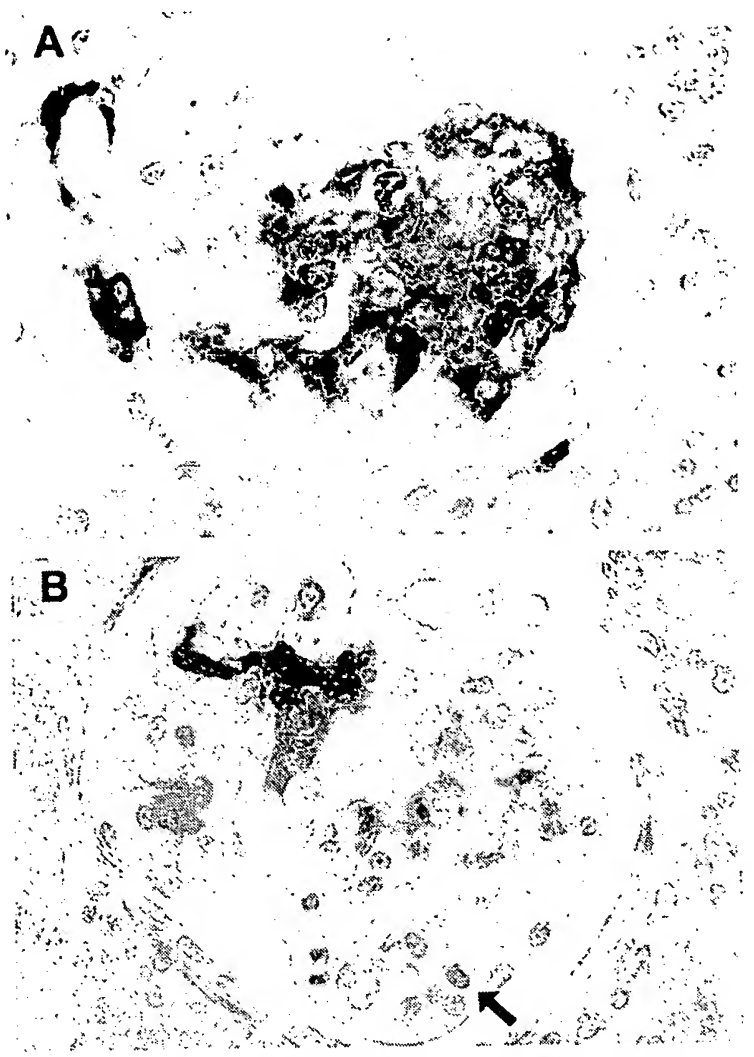

Figure 5. Effects of PDGF-B aptamer on glomerular mesangial cell proliferation as assessed by double immunostaining for nuclei incorporating the thymidine analogue BrdU and the mesangial cell *de novo* expression of α-smooth muscle actin on day 9 after disease induction. In a rat receiving scrambled DNA aptamer (A), marked glomerular *de novo* expression of α-smooth muscle actin (red stain) is noted, and at least three glomerular cells with a BrdU-positive nucleus (brown stain) exhibit an α-smooth muscle actin-positive cytoplasm, indicating that they are proliferating mesangial cells. In a rat receiving PDGF-B aptamer (B), little glomerular *de novo* expression of α-smooth muscle actin (red stain) is noted, and only one glomerular cell, which is α-smooth muscle actin negative, shows weak nuclear BrdU staining (arrow). Magnification, ×400.

was not due to masking of the PDGF B-chain epitope recognized by the anti-PDGF B-chain antibody, as the immunostaining intensity was not affected in renal sections that had been preincubated with the PDGF-B aptamer (immunostaining scores in sections preincubated with buffer, 2.70; with PDGF-B aptamer, 2.97; with scrambled aptamer, 2.78; means of two experiments each).

Reduction of Glomerular Monocyte/Macrophage Influx

The glomerular monocyte/macrophage influx was significantly reduced in the PDGF aptamer-treated rats as compared with rats receiving scrambled aptamer on days 6 and 9 after disease induction (Figure 4).

Effects on Proteinuria

Moderate proteinuria of up to 147 mg/24 hours was present on day 6 after disease induction in the three control groups (Figure 4). Treatment with the PDGF-B aptamer reduced the mean proteinuria on day 6, but this failed to reach statistical significance (Figure 4). Proteinuria on day 9 after disease induction was low and similar in all four groups (Figure 4).

Reduction of Glomerular Matrix Production and Accumulation

By immunohistochemistry, marked glomerular accumulation of type IV collagen and fibronectin was noted in all three control groups (Figure 6). The overexpression of both glomerular type IV collagen and fibronectin was significantly reduced in PDGF-B aptamer-treated rats (Figure 6). By *in situ* hybridization, the decreased glomerular protein expression of type IV collagen in PDGF-B aptamer-treated rats was shown to be associated with decreased glomerular synthesis of this collagen type (Figure 6). Sense controls for the *in situ* hybridizations were negative and similar to those published recently[25] (Figure 6E).

Discussion

In the anti-Thy-1.1 nephritis model, immunological damage to the mesangium, resulting in mesangiolysis, occurs during the first 24 to 48 hours after disease induction.[13,26] Subsequently, nondamaged mesangial cells immigrate from the extraglomerular mesangium and proliferate, giving rise to the pathological picture of mesangioproliferative glomerulonephritis.[7,27] Given this course of the nephritis, we initiated treatment on the 3rd day to avoid any interference of the therapy with pathomechanisms involved in disease induction, eg, glomerular binding of the nephritogenic antibody, complement activation, or cytotoxic damage, all of which peak during the 1st day of the disease. Furthermore, this experimental design enhances the clinical relevance of the study, as treatment was instituted after the onset of mesangioproliferative glomerulonephritis.

The major finding of the present study was that treatment with PDGF-B aptamer from days 3 to 9 after disease induction resulted in a near complete arrest of the overshooting mesangial cell proliferation and thereby led to a marked reduction of glomerular hypercellularity. Further support for the reduction of mesangial cell proliferation is provided by the observations that the glomerular *de novo* expression of α-smooth muscle actin and the overexpression of PDGF B-chain were also significantly inhibited by the PDGF-B aptamer. Both of these proteins are selectively up-regulated in activated mesangial cells in the anti-Thy-1.1 model,[15,24] and consequently, any intervention that reduces mesangial cell hyperplasia should also reduce expression of these proteins. It is of interest to note that mesangial cell proliferation as assessed by double immunostaining for BrdU and α-smooth muscle actin expression was reduced by 95% although glomerular mitoses were reduced by only 78% on day 9. This discrepancy suggests that proliferation of other glomer-

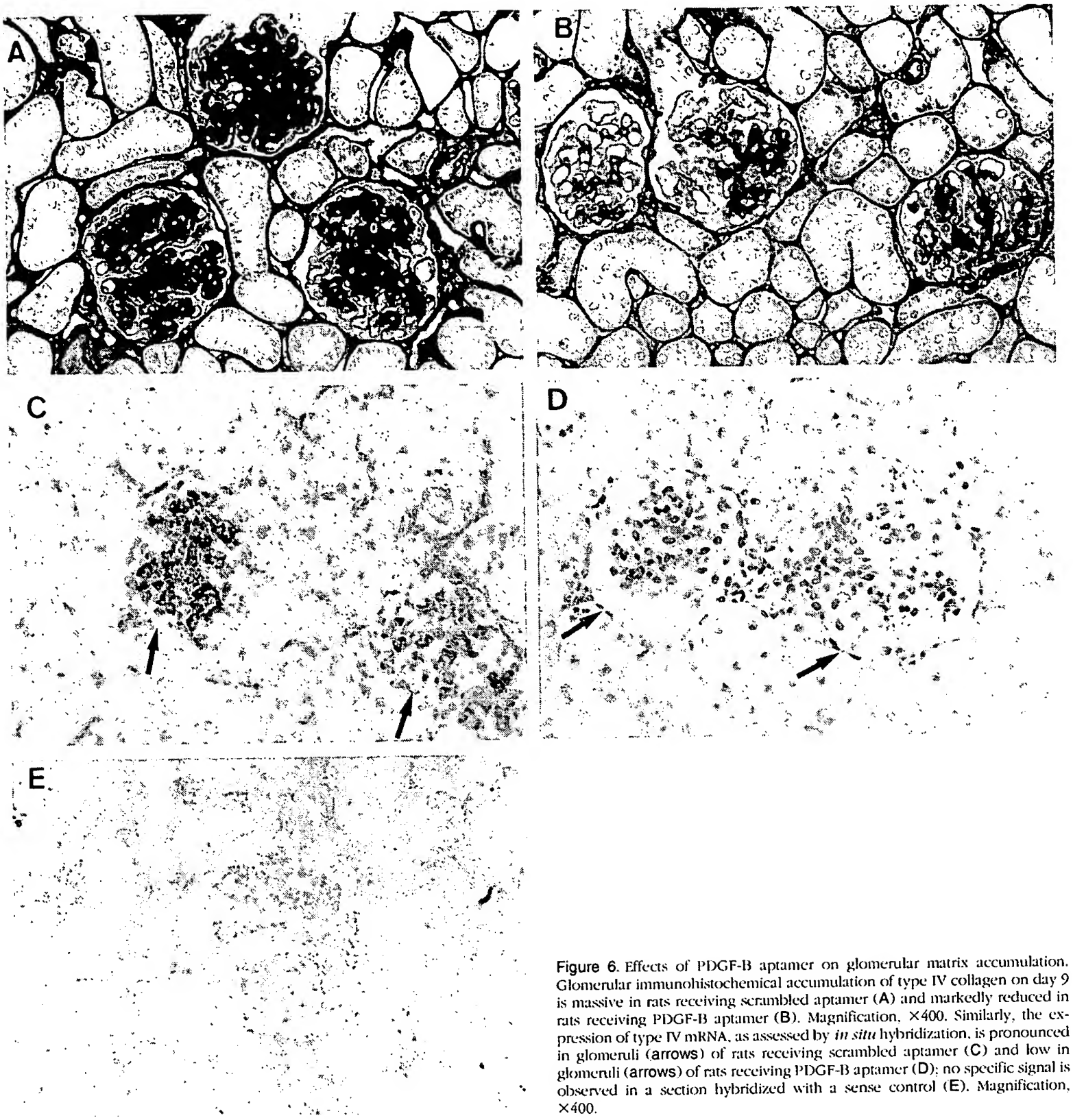

Figure 6. Effects of PDGF-B aptamer on glomerular matrix accumulation. Glomerular immunohistochemical accumulation of type IV collagen on day 9 is massive in rats receiving scrambled aptamer (**A**) and markedly reduced in rats receiving PDGF-B aptamer (**B**). Magnification, ×400. Similarly, the expression of type IV mRNA, as assessed by *in situ* hybridization, is pronounced in glomeruli (arrows) of rats receiving scrambled aptamer (**C**) and low in glomeruli (arrows) of rats receiving PDGF-B aptamer (**D**); no specific signal is observed in a section hybridized with a sense control (**E**). Magnification, ×400.

ular cells may be independent of PDGF (as demonstrated, for example, by the determination of proliferating monocytes/macrophages) and lends support to the highly specific action of the PDGF-B aptamer.

In addition to selectively abrogating mesangial cell proliferation, treatment with the PDGF-B aptamer also reduced the glomerular monocyte/macrophage influx and accumulation of extracellular matrix. Both of these latter processes are known to depend to a large degree on other cytokines produced by activated mesangial cells: glomerular macrophage influx on the production of monocyte chemoattractant protein-1[28] and matrix overproduction on the release of transforming growth factor-β.[29] The present data therefore suggest that PDGF B-chain is either linked to the mesangial cell production of these latter cytokines, as indicated by cell culture studies,[30] or that PDGF B-chain is directly and independently involved in chemotaxis and matrix production. Regardless of these issues, the present study establishes the release of PDGF B-chain as a central pathogenetic event in the development of mesangioproliferative glomerulonephritis. Our data also suggest that macrophage- or platelet-derived PDGF is unlikely to play a major role in the mediation of mesangioproliferative changes in this model, as influx of both cell types peaks at ~24 hours,[13] ie, 2 days before the initiation of anti-PDGF treatment.

Similar, albeit quantitatively somewhat lower, effects were also noted in our previous study with a neutralizing antibody to PDGF B-chain in the anti-Thy-1.1 nephritis model; treatment resulted in a 57% reduction of glomerular cell proliferation on day 4 and reduced glomerular matrix accumulation by approximately one score point.[6] One important concern in that study was that large amounts of IgG (600 mg/kg/day), both neutralizing anti-PDGF antibody and control IgG, had to be administered on a daily basis to the rats. Large doses of IgG can ameliorate the course of immune-mediated renal disease,[31] and the therapeutic effect of IgG *per se* is variable from batch to batch (R. J. Johnson and J. Floege, personal observation). Second, mesangial cells express Fc-γ receptors and modulate their cytokine release on binding of IgG to Fc receptors.[10] These observations, in addition to the immunogenicity of heterologous antibodies, impose considerable restrictions on the interpretation of such studies.

At present, no other specific PDGF B-chain antagonists have been tested *in vivo*. Trapidil, an anti-platelet agent, has been shown to interfere with PDGF B-chain binding to mesangial PDGF receptors, but its action is not specific for PDGF.[32] Preliminary data suggest that a blocker of the PDGF receptor-associated tyrosine kinase may also ameliorate the course of mesangioproliferative nephritis,[33] but again, the compound was not specific for PDGF and also reduced, for example, basic-FGF-induced cell proliferation.

The possibility to develop aptamer antagonists for defined biological mediators has become an attractive novel therapeutic approach in various diseases.[23] These previous studies, in which thrombin, selectins, and neutrophil elastase were targeted, have demonstrated the ability of aptamers to act as antagonists of plasma or leukocyte proteins *in vivo*.[34–36] The present study is the first to demonstrate that specific antagonism of peptide growth factors, which are produced in a spatially much more confined manner, by high-affinity aptamers *in vivo* is not only feasible but also highly effective. In pilot studies the high effectiveness of the PDGF-B aptamer was also demonstrated in an experiment in which the injection of 5 mg of the aptamer at a single time point, ie, day 3 of the nephritis, was as efficient as several days of twice-daily treatment with a total of 10 to 30 mg (unpublished data). Furthermore, in pilot experiments we have observed that the effects of the PDGF-B aptamer *in vivo* are dose dependent and can be demonstrated with doses as low as 2 mg total. In support of our findings, the PDGF aptamer used in this study has recently exhibited efficacy in the rat model of restenosis (C.-H. Heldin and A. Östman, personal communication).

Apart from their specificity and potency, the use of aptamers largely circumvents problems of Fc receptor binding. Furthermore, although the effort to thoroughly examine the immunogenicity of aptamers is still in progress, extensive *in vivo* data obtained to date suggest that aptamers induce little if any immune response (J. Bill and G. Biesecker, unpublished results). Another attractive feature of aptamers is that their pharmacokinetic behavior can easily be altered, for example, by altering the molecular size (eg, via variation of the length of the attached PEG), hydrophobicity (eg, via packaging them in or on liposomes[9]), or other features. A potential problem with the use of nucleic-acid-based antagonists is their polyanionic character, which might in itself affect the course of diseases. Thus, other polyanionic compounds, for example, heparins or heparan sulfate proteoglycans, are also effective in reducing mesangial cell proliferation in the anti-Thy-1.1 nephritis model.[14] However, in the present study, this concern was resolved by the ineffectiveness of a scrambled aptamer, which is identical in composition and predicted secondary structure to the PDGF-B aptamer but whose binding affinity for PDGF B-chain is dramatically lower.

In conclusion, we describe the efficacy of a high-affinity nucleic-acid-based growth factor antagonist *in vivo* and thereby extend the currently available evidence that PDGF B-chain is a central mediator in mesangioproliferative glomerulonephritis. The specificity and effectiveness demonstrated with the currently used aptamer opens the possibility for growth factor inhibition over prolonged periods. Aptamers may thus be used both to elucidate the role of individual growth factors that represent potential targets for therapeutic intervention and to serve as drug candidates for the treatment of disease states characterized by growth factor overexpression.

Acknowledgments

The technical help of Monika Kregeler, Astrid Fitter, and Yvonne Schönborn is gratefully acknowledged. We thank Jeff Walenta, Philippe Bridonneau, Girija Rajagopal, and Tim Romig for the synthesis and purification of aptamers. We also thank Nikos Pagratis and Dan Drolet for cloning of rat PDGF-BB and Joe Senello for providing rat serum for the aptamer stability studies.

References

1. Tuerk C, Gold L: Systematic evolution of ligands by exponential enrichment: RNA ligands to bacteriophage T4 DNA polymerase. Science 1990, 249:505–510
2. Ellington A, Szostak J: In vitro selection of RNA molecules that bind specific ligands. Nature 1990, 346:818–822
3. Ross R: Cell biology of atherosclerosis. Annu Rev Physiol 1995, 57:791–804
4. Floege J, Johnson RJ: Multiple roles for platelet-derived growth factor in renal disease. Miner Electrolyte Metab 1995, 21:271–282
5. Slomowitz LA, Klahr S, Schreiner GF, Ichikawa I: Progression of renal disease. N Engl J Med 1988, 319:1547–1548
6. Johnson RJ, Raines EW, Floege J, Yoshimura A, Pritzl P, Alpers C, Ross R: Inhibition of mesangial cell proliferation and matrix expansion in glomerulonephritis in the rat by antibody to platelet-derived growth factor. J Exp Med 1992, 175:1413–1416
7. Floege J, Eng E, Young BA, Johnson RJ: Factors involved in the regulation of mesangial cell proliferation in vitro and in vivo. Kidney Int Suppl 1993, 39:S47–S54
8. Green LS, Jellinek D, Jenison R, Östman A, Heldin CH, Janjić N: Inhibitory DNA ligands to platelet-derived growth factor B-chain. Biochemistry 1996, 35:14413–14424
9. Willis MC, Collins BD, Zhang T, Green LS, Sebesta D, Bell C, Kellogg E, Gill SC, Magillanez A, Knauer S, Bendele RA, Gill PS, Janjić N: Liposome-anchored vascular endothelial growth factor aptamers. Bioconj Chem 1998, 9:573–582
10. Radeke HH, Gessner JE, Uciechowski P, Magert HJ, Schmidt RE,

Resch K: Intrinsic human glomerular mesangial cells can express receptors for IgG complexes (hFcγRIII-A) and the associated FcεRI γ-chain. J Immunol 1994, 153:1281–1292
11. Floege J, Topley N, Hoppe J, Barrett TB, Resch K: Mitogenic effect of platelet-derived growth factor in human glomerular mesangial cells: modulation and/or suppression by inflammatory cytokines. Clin Exp Immunol 1991, 86:334–341
12. Lonnemann G, Shapiro L, Engler Blum G, Muller GA, Koch KM, Dinarello CA: Cytokines in human renal interstitial fibrosis. I. Interleukin-1 is a paracrine growth factor for cultured fibrosis-derived kidney fibroblasts. Kidney Int 1995, 45:837–844
13. Johnson RJ, Garcia RL, Pritzl P, Alpers CE: Platelets mediate glomerular cell proliferation in immune complex nephritis induced by antimesangial cell antibodies in the rat. Am J Pathol 1990, 136:369–374
14. Burg M, Ostendorf T, Mooney A, Koch KM, Floege J: Treatment of experimental mesangioproliferative glomerulonephritis with non-anticoagulant heparin: therapeutic efficacy and safety. Lab Invest 1997, 76:505–516
15. Yoshimura A, Gordon K, Alpers CE, Floege J, Pritzl P, Ross R, Couser WG, Bowen-Pope DF, Johnson RJ: Demonstration of PDGF B-chain mRNA in glomeruli in mesangial proliferative nephritis by in situ hybridization. Kidney Int 1991, 40:470–476
16. Kliem V, Johnson RJ, Alpers CE, Yoshimura A, Couser WG, Koch KM, Floege J: Mechanisms involved in the pathogenesis of tubulointerstitial fibrosis in 5/6-nephrectomized rats. Kidney Int 1996, 49:666–678
17. Hugo C, Pichler R, Gordon K, Schmidt R, Amieva M, Couser WG, Furthmayr H, Johnson RJ: The cytoskeletal linking proteins, moesin and radixin, are upregulated by platelet-derived growth factor, but not basic fibroblast growth factor in experimental mesangial proliferative glomerulonephritis. J Clin Invest 1996, 97:2499–2508
18. Eitner F, Westerhuis R, Burg M, Weinhold B, Gröne HJ, Ostendorf T, Rüther U, Koch KM, Rees AJ, Floege J: Role of interleukin-6 in mediating mesangial cell proliferation and matrix production in vivo. Kidney Int 1997, 51:69–78
19. Pieken WA., Olsen DB, Benseler F, Aurup H, Eckstein F: Kinetic characterization of ribonuclease-resistant 2′-modified hammerhead ribozymes. Science 1991, 253:314–317
20. Cummins LL, Owens SR, Risen LM, Lesnik EA, Freier SM, McGee D, Guinosso CJ, Cook PD: Characterization of fully 2′-modified oligoribonucleotide hetero- and homoduplex hybridization and nuclease sensitivity. Nucleic Acids Res 1995, 23:2019–2024
21. Herren B, Weyer KA, Rouge M, Lötscher P, Pech M: Conservation in sequence and affinity of human and rodent PDGF ligands and receptors. Biochim Biophys Acta 1993, 1173:294–302
22. Lindner V, Giachelli CM, Schwartz SM, Reidy MA: A subpopulation of smooth muscle cells in injured rat arteries expresses platelet-derived growth factor B-chain. Circ Res 1995, 76:951–957
23. Gold L, Polisky B, Uhlenbeck OC, Yarus M: Diversity of oligonucleotide functions. Annu Rev Biochem 1995, 64:763–797
24. Johnson RJ, Iida H, Alpers CE, Majesky MW, Schwartz SM, Pritzl P, Gordon K, Gown AM: Expression of smooth muscle cell phenotype by rat mesangial cells in immune complex nephritis: alpha-smooth muscle actin is a marker of mesangial cell proliferation. J Clin Invest 1991, 87:847–858
25. Canaan-Kühl S, Ostendorf T, Zander K, Koch KM, Floege J: C-natriuretic peptide inhibits mesangial cell proliferation and matrix accumulation in vivo. Kidney Int 1998, 53:1143–1151
26. Yamamoto T, Wilson CB: Quantitative and qualitative studies of antibody-induced mesangial cell damage in the rat. Kidney Int 1987, 32:514–525
27. Hugo C, Shankland SJ, Bowen-Pope DF, Couser WG, Johnson RJ: Extraglomerular origin of the mesangial cell after injury. J Clin Invest 1997, 100:786–794
28. Fujinaka H, Yamamoto T, Takeya M, Feng L, Kawasaki K, Yaoita E, Kondo D, Wilson CB, Uchiyama M, Kihara I: Suppression of anti-glomerular basement membrane nephritis by administration of anti-monocyte chemoattractant protein-1 antibody in WKY rats. J Am Soc Nephrol 1997, 8:1174–1178
29. Border WA, Okuda S, Languino LR, Sporn MB, Ruoslahti E: Suppression of experimental glomerulonephritis by antiserum against transforming growth factor-β1. Nature 1990, 346:371–374
30. Goppelt-Struebe M, Stroebel M: Synergistic induction of monocyte chemoattractant protein-1 by platelet-derived growth factor and interleukin-1. FEBS Lett 1995, 374:375–378
31. Nangaku M, Pippin J, Richardson CA, Schulze M, Young BA, Alpers CE, Gordon KL, Johnson RJ, Couser WG: Beneficial effects of systemic immunoglobulin in experimental membranous nephropathy. Kidney Int 1996, 50:2054–2062
32. Gesualdo L, DiPaolo S, Ranieri E, Schena FP: Trapidil inhibits human mesangial cells proliferation: effect on PDGF β-receptor binding and expression. Kidney Int 1994, 46:1002–1009
33. Yagi M, Kato S, Kobayashi Y, Kobayashi N, Iinuma N, Nagano N, Yamamoto T: Beneficial effects of a selective platelet-derived growth factor receptor autophosphorylation inhibitor on proliferative glomerulonephritis in the rats. J Am Soc Nephrol 1997, 8:488A
34. Griffin LC, Tidmarsh GF, Bock LC, Toole JJ, Leung LLK: In vivo anticoagulant properties of a novel nucleotide-based thrombin inhibitor and demonstration of regional anticoagulation in extracorporeal circuits. Blood 1993, 81:3271–3276
35. Hicke B J, Watson SR, Koenig A, Lynott CK, Bargatze RF, Chang YF, Ringquist S, Moon-McDermott L, Jennings S, Fitzwater T, Han HL, Varki N, Albinana I, Willis MC, Varki A, Parma D: DNA aptamers block L-selectin function in vivo. J Clin Invest 1996, 98:2688–2692
36. Bless NM, Smith D, Charlton J, Czermak BJ, Schmal H, Friedl HP, Ward PA: Protective effects of an aptamer inhibitor of neutrophil elastase in lung inflammatory injury. Curr Biol 1997, 7:877–880

Bioconjugate Chem. 1998, *9*, 573–582

Liposome-Anchored Vascular Endothelial Growth Factor Aptamers[§]

Michael C. Willis,*,† Brian Collins,‡ Tong Zhang,‡ Louis S. Green,† David P. Sebesta,† Carol Bell,† Elizabeth Kellogg,† Stanley C. Gill,† Anna Magallanez,† Susan Knauer,† Ray A. Bendele,† Parkash S. Gill,‡ and Nebojša Janjić*,†

NeXstar Pharmaceuticals, 2860 Wilderness Place, Boulder, Colorado 80301, and Norris Cancer Hospital, School of Medicine, University of Southern California, Los Angeles, California 90033. Received January 7, 1998; Revised Manuscript Received April 30, 1998

Nuclease-resistant aptamers identified from randomized nucleic acid libraries represent a novel class of drug candidates. Aptamers are synthesized chemically and therefore can be readily modified with functional groups that modulate their properties. We report here on the preparation, initial characterization, and functional properties of a nuclease-resistant vascular endothelial growth factor (VEGF) aptamer anchored in liposome bilayers through a lipid group on the aptamer. While the high-affinity binding to VEGF is maintained, the plasma residence time of the liposome-anchored aptamer is considerably improved compared with that of the free aptamer. The lipid group attachment and/or liposome anchoring leads to a dramatic improvement in inhibitory activity of the aptamer toward VEGF-induced endothelial cell proliferation in vitro and vascular permeability increase and angiogenesis in vivo.

INTRODUCTION

Nucleic acids are capable of folding into stable and intricate three-dimensional structures. Randomized nucleic acid libraries therefore contain molecules with many shapes in which functional groups capable of hydrogen bonding, hydrophobic, and charge–charge interactions are arranged in a defined spatial orientation. By taking advantage of iterative cycles of affinity selection and amplification, the SELEX[1] process has emerged in recent years as a highly efficient method of identifying rare nucleic acid ligands (aptamers) from random libraries that bind to other molecules with high affinity and specificity (*1*–*4*). The advent of nuclease-stabilized libraries, such as the 2′-amino- or 2′-fluoropyrimidine RNA, has recently increased the utility of the SELEX process as a tool for identifying drug candidates (*5*–*8*).

We have recently used the SELEX process to identify 2′-aminopyrimidine RNA aptamers that bind to vascular endothelial growth factor (VEGF) (*9*), a potent inducer of angiogenesis. Angiogenesis, the growth of new blood vessels from existing vessels, accompanies physiological processes such as wound healing and reproductive cycles and is tightly controlled in healthy adults by opposing effects of positive and negative regulators. Under certain pathological conditions, including proliferative retinopathies, rheumatoid arthritis, psoriasis, and cancer, positive regulators prevail and angiogenesis contributes to disease progression (reviewed in ref *10*). VEGF is unique among angiogenic growth factors described to date in that it specifically stimulates endothelial cell proliferation (*11*–*13*) and induces a transient increase in blood vessel permeability with respect to macromolecules (hence, its alternative and original name, vascular permeability factor) (*14*–*16*). Increased vascular permeability and the resulting deposition of plasma proteins in the extravascular space assist the new vessel formation by providing a provisional matrix for the migration of endothelial cells (*17*). Hyperpermeability is indeed a characteristic feature of new vessels (*17*). In addition, compensatory angiogenesis induced by tissue hypoxia is now known to be mediated by VEGF (*18*, *19*). Most tumors and tumor cell lines are capable of producing and secreting VEGF, and inhibition of VEGF activity leads to the reduced rate of tumor growth as well as the reduced incidence of metastases. Together, these observations have led to the assertion that VEGF is the crucial positive regulator of angiogenesis (*20*, *21*). VEGF is a secreted disulfide-linked homodimer that occurs in four forms (VEGF-121, VEGF-165, VEGF-189, and VEGF-206) as a result of alternative splicing of the VEGF gene, with VEGF-165 being the most abundantly occurring form (*22*, *23*). The biological effects of VEGF are mediated through two tyrosine kinase receptors (Flt-1 and Flk-1/KDR) whose expression is highly restricted to cells with endothelial and hematopoietic origins (*24*–*27*).

In the 2′-aminopyrimidine RNA aptamer, the subnanomolar binding affinity for VEGF-165 is encoded in a sequence of 24 nucleotides (*9*). We have achieved additional resistance to nuclease degradation by adding short phosphorothioate caps at the 3′ and 5′ ends and by substituting 2′-*O*-methylpurine nucleotides at all purine positions (10 out of 14) that tolerate such a substitution without loss of binding affinity. Such an aptamer (NX213 = 5′-dT*dT*dT*dT*mAaCaCaCaUrGrAaUmGrGaUmAmGrAaCmGaCaCmGmG mGmGaUmGdT*dT*dT*dT*dT-3′, where prefixes d, r, a, and m denote deoxy-, ribodeoxy-, 2′-amino-, and 2′-*O*-methylnucleotides and a superscript

§ This paper is dedicated to Prof. Y. Pocker on the occasion of his 70th birthday.

* Address correspondence to these authors.
† NeXstar Pharmaceuticals.
‡ University of Southern California.

[1] Abbreviations: AUC, area under the curve; CAM, chorioallantoic membrane; DAG–NX213-L, liposome-anchored DAG-modified VEGF aptamer; DAG–NX213, DAG-modified VEGF aptamer; DAG–scNX213-L, liposome-anchored DAG–scNX213; DAG–scNX213, DAG-modified scNX213; DAG, dialkylglycerol; DSPC, distearoylphosphatidylcholine; NX213, 2′-aminopyrimidine RNA VEGF aptamer; PBS, phosphate-buffered saline; scNX213, sequence-scrambled analogue of the VEGF aptamer; SELEX, systematic evolution of ligands by exponential enrichment; VEGF, vascular endothelial growth factor.

S1043-1802(98)00002-0 CCC: $15.00
Published on Web 07/10/1998

s denotes phosphorpthioate internucleoside linkages) inhibited the binding of [^{125}I]VEGF to receptors expressed on human umbilical vein endothelial cells (HUVECs) with an EC_{50} of ≈1 nM, suggesting that the aptamer could be an inhibitor of VEGF-mediated effects (*9*). However, compared to its very good stability in biological fluids in vitro (*9*), the residence time of NX213 in plasma in vivo was found to be very short (see below), mostly as a consequence of rapid renal clearance (S. C. Gill and R. Fielding, unpublished results). Since aptamers in the 20−35-nucleotide size range have molecular masses of ≈7−12 kDa, one obvious way of increasing their plasma residence times is by associating them with large, inert entities. Liposomes represent a class of supramolecular assemblies that could be used for this purpose. We report here on the synthesis and initial characterization of a lipid (dialkylglycerol, DAG) derivative of the VEGF aptamer (DAG−NX213) in which the lipid group is used to anchor the aptamers in liposome bilayers. The preparation of liposome-anchored aptamers is essentially as straightforward as the preparation of unloaded liposomes. Importantly, both the addition of the DAG group and liposome anchoring do not interfere with the ability of the aptamer to bind to VEGF with a high affinity. The plasma residence time of the liposome-anchored aptamer (DAG−NX213-L) is considerably longer than that of NX213. We also show that DAG−NX213 and/or DAG−NX213-L exhibit enhanced inhibitory activity compared with the free aptamer toward VEGF-induced endothelial cell proliferation in vitro and vascular permeability increase and CAM angiogenesis in vivo.

EXPERIMENTAL PROCEDURES

Preparation of the DAG Phosphoramidite Reagent. *Tetraethylene Glycol Monotosylate (2).* Tetraethylene glycol (200 mL, 1.15 mol) was dissolved in 500 mL of pyridine, cooled to 0 °C, and treated with 22.0 g (0.115 mol) of *p*-toluenesulfonyl chloride. Once the solution was formed, the reaction mixture was stored in the refrigerator overnight, and then concentrated in vacuo. The residue was dissolved in 800 mL of EtOAc and extracted with 3 × 600 mL of H_2O. The H_2O fractions were back-extracted with EtOAc, and the combined EtOAc fractions were extracted with saturated aqueous Na_2HPO_4. The organic phase was dried over $MgSO_4$ and concentrated to a colorless oil. The oil was purified by flash chromatography using 800 mL of silica gel and eluting with hexane, then 25% EtOAc/50% EtOAc in hexane, then EtOAc, and then 10% MeOH/20% MeOH in EtOAc to afford 23.7 g (60%) of pure product and 11% of product containing a minor impurity: ^{1}H NMR (300 MHz, $CDCl_3$) δ 7.77 (d, J = 8.1 Hz, 2H), 7.32 (d, J = 8.1 Hz, 2H), 4.13 (t, J = 4.8 Hz, 2H), 3.68−3.53 (m, 14H), 2.58 (t, J = 5.6 Hz, 1H), 2.42 (s, 3H); ^{13}C NMR (75 MHz, $CDCl_3$) δ 168.2, 158.3, 144.8, 135.9, 133.8, 132.0, 129.9, 128.0, 127.7, 126.6, 123.1, 113.0, 85.9, 73.0, 70.6, 70.4, 70.0, 69.7, 67.8, 64.4, 55.1, 37.1; low-resolution MS *m/z* calculated for $C_{15}H_{24}O_5S$ (M + 1) 349.1 Da.

Tetraethylene Glycol Monophthalimide (3). To a stirred solution of 31.96 g (0.092 mol) of **2** in 400 mL of anhydrous DMF were added 14.2 g (1.05 equiv) of phthalimide and 14.4 mL (1.05 equiv) of 1,8-diazabicyclo-[5.4.0]undec-7-ene. The solution was heated at 70 °C for 18 h and then concentrated in vacuo. The crude yellow oil was purified by flash chromatography using 1600 mL of silica gel and eluting with 25% EtOAc/50% EtOAc/75% EtOAc in hexane, then EtOAc, and then 10% MeOH/20% MeOH in EtOAc to afford 23.8 g (80%) of **3** as an oil. Upon standing, **3** became a waxy white solid: ^{1}H NMR (300 MHz, $CDCl_3$) δ 7.84−7.78 (m, 2H), 7.70−7.66 (m, 2H), 3.86 (t, J = 5.6 Hz, 2H), 3.70 (t, J = 5.6 Hz, 2H), 3.64−3.51 (m, 12H), 2.67 (bs, 1H); ^{13}C NMR (75 MHz, $CDCl_3$) δ 168.2, 133.8, 132.0, 123.1, 72.4, 70.5, 70.4, 70.2, 70.0, 67.8, 61.6, 37.2.

Synthesis of Compound 4. A solution of 15 g (0.0464 mol) of **3** in 150 mL of THF and 15 mL of DMF was cooled to 0° C under Ar. Allyl bromide (6.0 mL, 1.5 equiv) was added to the solution, followed by addition of 1.76 g (1.5 equiv) of NaH as a solid. The opaque yellow suspension was stirred at 0 °C for 30 min and then at room temperature for 18 h. MeOH (50−100 mL) was added, and the mixture was concentrated in vacuo. The crude material was purified by flash chromatography using 1500 mL of silica gel and eluting with 25% EtOAc/50% EtOAc/75% EtOAc in hexane, then EtOAc, and then 10% MeOH in EtOAc to afford 11.05 g (65%) of **4** as a yellow oil: ^{1}H NMR (300 MHz, $CDCl_3$) δ 7.84−7.80 (m, 2H), 7.72−7.67 (m, 2H), 5.94−5.84 (m, 1H), 5.28−5.14 (m, 2H), 3.99 (d, J = 5.61 Hz, 2H), 3.88 (t, J = 5.85 Hz, 2H), 3.72 (t, J = 5.76 Hz, 2H), 3.64−3.54 (m, 13H); ^{13}C NMR (75 MHz, $CDCl_3$) δ 168.0, 134.6, 133.7, 131.9, 123.0, 116.9, 72.0, 70.4, 69.9, 69.2, 67.7, 37.0.

1-(Dimethoxytrityl)-3-(phthalimidotetraethylene glycolyl)-rac-glycerol (5). To a stirred solution of **4** (10.13 g, 0.0279 mol) in 100 mL of acetone and 1 mL of H_2O was added 3.98 g (1.22 equiv) of *N*-methylmorpholine *N*-oxide. To this suspension was added 1.75 mL (0.005 equiv) of OsO_4 as a 2.5% solution in ^{t}PrOH. After addition of the OsO_4 solution, the reaction mixture became clear yellow. After TLC analysis indicated complete conversion of **4** (ca. 16 h), the reaction mixture was treated with 1.5 g of sodium hydrosulfite and 5.0 g of florisil and stirred for 30 min. The suspension was filtered through florisil, and the filtrate was concentrated to an oil. This crude product was combined with another batch prepared in the same manner from 1.0 g of **4**. Two 100 mL portions of pyridine were coevaporated from the combined lots, and the residue was dissolved in 300 mL of pyridine. The solution was cooled to 0 °C, and 10.89 g (1.05 equiv) of 4,4′-dimethoxytrityl chloride was added. A drying tube was placed into the flask, and the reaction mixture was stirred at room temperature for 16 h. The solution was treated with 20 mL of MeOH and concentrated in vacuo, keeping the temperature of the water bath below 40 °C. The crude oil was purified by flash chromatography using 1100 mL of silica gel (wet-packed onto the column using 3% triethylamine in hexane) and eluting with 10−100% EtOAc in hexane (all containing 3% triethylamine) to give 21.3 g (89% after two steps) of **5** as a yellow oil: ^{1}H NMR (300 MHz, $CDCl_3$) δ 7.80−7.77 (m, 2H), 7.66−7.64 (m, 2H), 7.39−7.22 (m, 9H), 7.20−6.76 (m, 4H), 3.97 (bs, 1H), 3.84 (t, J = 5.97 Hz, 2H), 3.74 (s, 6H), 3.68 (t, J = 5.7 Hz, 2H), 3.60−3.49 (m, 14H), 3.13−2.76 (m, 2H), 2.00 (bs, 1H); ^{13}C NMR (75 MHz, $CDCl_3$) δ 168.2, 158.3, 144.8, 135.9, 133.8, 132.0, 129.9, 128.0, 127.7, 126.6, 123.1, 113.0, 85.9, 73.0, 70.6, 70.4, 70.0, 69.7, 67.8, 64.4, 55.1, 37.1; low-resolution MS *m/z* calculated for $C_{40}H_{45}O_{10}N$ (M + NH_4^+) 717.5 Da.

1-(Dimethoxytrityl)-3-(aminotetraethylene glycolyl)-sn-glycerol (6). Compound **5** (5.2 g, 7.2 mmol) was taken up in 50 mL of 40% methylamine in H_2O, and 10 mL of methanol was added to solublize the starting material. The reaction mixture was heated at 50 °C for 5 h and then concentrated in vacuo and coevaporated with toluene. The crude material was purified by flash chromatography on 200 mL of silica gel, eluting with 15% methanolic ammonia in dichloromethane. **6** (3.94 g, 96%) was collected as a pale yellow oil: ^{1}H NMR (300 MHz,

$CDCl_3$) δ 7.46–7.21 (m, 9H, DMT), 6.81 (d, 4H, DMT), 4.00 (m, 1H), 3.80 (s, 6H), 3.70–3.49 (overlapping m, 18H), 3.20 (dd, J = 9.24, 5.49 Hz, 1H), 3.12 (dd, J = 9.21, 6.0 Hz, 1H), 2.84–2.80 (m, 3H); ^{13}C NMR (75 MHz, $CDCl_3$) δ 158.30, 144.82, 136.01, 129.95, 128.04, 127.66, 126.61, 112.95, 85.85, 73.46, 72.85, 70.55, 70.45, 69.99, 69.51, 64.43, 55.10, 41.40; low-resolution MS *m/z* calculated for $C_{32}H_{44}O_8N$ ($M + 1^+$) 570.353 Da, found 570.4 Da.

Chloroformate 7. To a stirred solution of 3 g (5.03 mmol) of 1,2-di-*O*-octadecyl-*sn*-glycerol in 60 mL of toluene was added 20 mL of a 1.93 M solution of phosgene. Additional phosgene solution (2 × 10 mL, total of 15.4 equiv of phosgene) was added until no further alcohol starting material remained (by ^{1}H NMR analysis of concentrated aliquots). The excess phosgene and HCl was removed with an aspirator, and the reaction mixture was concentrated in vacuo to afford 3.3 g (98%) of the desired chloroformate **7** as a white powder: ^{1}H NMR (300 MHz, $CDCl_3$) δ 4.45 (dd, J = 11.22, 3.69 Hz, 1H), 4.34 (dd, J = 11.22, 6.15 Hz, 1H), 3.65 (m, 1H), 3.56–3.40 (m, 6H), 1.53 (m, 4H), 1.24 (m, 62H), 0.87 (t, J = 6.36 Hz, 6H); ^{13}C NMR (75 MHz, $CDCl_3$) δ 75.90, 71.91, 71.35, 70.93, 69.36, 31.99, 29.96–29.44 (overlapping signals from hydrocarbon chains), 26.13, 26.04, 22.76, 14.18.

Conjugate 8. To a stirred solution of 2.25 g (3.95 mmol) of **6** in 60 mL of pyridine was added 2.6 g of the distearyl glycerol chloroformate **7**. ^{1}H NMR analysis of a concentrated aliquot after 2 h revealed no remaining chloroformate, and the mixture was concentrated in vacuo. The crude residue was combined with material similarly prepared from 0.5 g (0.88 mmol) of **6** and 0.58 g of the chloroformate **7**, and the combined lots were purified by flash silica gel chromatography on a column of 100 mL of silica gel (packed in hexanes containing 2% triethylamine) eluting with 200 mL hexanes, and then 250 mL each of 10–20 and 30% EtOAc in hexanes and 500 mL of 40% EtOAc in hexanes, then 250 mL each of 50, 60, 70, and 80% EtOAc in hexanes, and finally with 250 mL of EtOAc. The product-containing fractions were concentrated to afford 3.3 g (57%) of the conjugate **8**.

Phosphoramidite 9. To a stirred solution of 3.8 g (3.26 mmol) of conjugate **8** in 25 mL of CH_2Cl_2 were added 1.14 mL (6.52 mmol) of diisopropylethylamine and then 1.09 mL (4.88 mmol) of 2-cyanoethyl *N,N*-diisopropylchlorophosphoramidite. After 2 h, the mixture was diluted with CH_2Cl_2 and washed with a saturated $NaHCO_3$ solution, dried over Na_2SO_4, and concentrated, The crude residue was purified by flash silica gel chromatography on a column of 125 mL of silica gel (packed in hexanes containing 2% triethylamine) eluting with 100 mL hexanes, then 250 mL each of 10 and 20% EtOAc in hexanes and 500 mL of 30% EtOAc in hexanes, and then 250 mL of 50% EtOAc in hexanes. The product-containing fractions were concentrated to afford 4.2 g (95%) of the phosphoramidite **9**: ^{31}P NMR ($CDCl_3$) δ 151.[illegible], 151.08.

Preparation of DAG–Aptamers. The VEGF aptamer (NX213) and its scrambled analogue (scNX213) were prepared by standard solid phase oligonucleotide synthesis protocols as described (ref *9* and references therein). For DAG-conjugated aptamers, phosphoramidite **9** dissolved in CH_2Cl_2 (acetonitrile was not an adequate solvent) was added as the last coupling step to the 5′ end of the aptamers (two 30 min coupling cycles using a 4-fold excess of the amidite; coupling efficiency ≈ 90%, by dimethoxytrityl absorbance). The DAG–aptamer was purified by reverse phase HPLC (PRP-1 column, Hamiltom, Reno, NV) using a 100 mM triethylammonium acetate/acetonitrile gradient followed by desalting and salt (Na^+ for triethylammonium) exchange (PRP-1 column). Following purification, >99% of the oligonucleotide contained the DAG moiety. Electrospray mass spectroscopic analysis of DAG–NX213 indicated two major components with *m/z* values of 11 714.2 and 11 699.2 Da (calculated mass of DAG–NX213 = 11 715.3 Da). The *m/z* 11 699.2 Da component (≈16 Da less than calculated) is probably due to incomplete oxidation by the sulfurizing reagent (Glen Research, Sterling, VA), resulting on average in seven instead of eight phosphorothioate internucleoside linkages per molecule.

Preparation of Liposome-Associated Aptamers. A spray-dried mixture of 1,2-distearoyl-*sn*-glycero-3-phosphatidylcholine (DSPC) and cholesterol (2 mol:1 mol) was placed in a 14 mL Pyrex glass centrifuge tube (50 mg of total lipid) and suspended in a 1 mL solution containing 1 mg/mL (0.12 mol %) DAG–NX213 or DAG–scNX213 in 9% sucrose buffered to pH 7.4 with 25 mM sodium phosphate. The lipid suspension was incubated for 5–15 min at 65 °C, gently mixed until evenly suspended, and sonicated with a 0.125 in. microtip probe at 65 °C with an approximately 215 W input power using a model 475 Virsonic power supply (Virtis, Gardiner, NY). The progress of the sonication was followed by particle sizing using dynamic light scattering (Leeds Northrop MicroTrac Model 150 Particle Analyzer, Honeywell, Ft. Washington, PA). Liposome sizing was determined by the volume of distribution method using the manufacturer's protocol (MicroTrac). Sonication was typically stopped when the liposomes reached an essentially unimodal distribution with a mean vesicle diameter of approximately 50–65 nm. The final liposome product is sterilized by filtration through a 0.2 μm syringe filter (Supor Acrodisc 25, Gelman Sciences, Ann Arbor, MI). The total concentration of aptamer in the liposomal formulation was determined from the absorbance value at 260 nm (ϵ_{260} = 27 au mg^{-1} mL^{-1}) in a 0.1% sodium dodecyl sulfate solution. In all experiments with the liposome-anchored aptamer, the total aptamer concentration was used without a correction for the orientation of the aptamer in the liposome bilayer (see below).

Ribonuclease T_1 Digestion of the Free and Liposomal Aptamers. All digests were performed with ^{32}P 3′ end-labeled DAG–NX213 at 8 pmol/μL and 20 units/μL RNase T_1 in 25 mM sodium phosphate buffer (pH 7.4) containing 9% sucrose. The digests were terminated by adding an equal volume of gel loading solution (80% formamide, 89 mM Tris borate, 1 mM EDTA, 2% sodium dodecyl sulfate, and 0.7 M β-mercaptoethanol), followed by heating at 95 °C for 2 min and cooling on ice before loading on a 20% polyacrylamide/7 M urea gel.

Plasma Pharmacokinetics. The pharmacokinetic properties of VEGF aptamers NX213, DAG–NX213, and DAG–NX213-L were determined in Sprague-Dawley rats. In each study, the aptamer was diluted in PBS to a concentration of 1.0 mg/mL on the basis of UV absorption at 260 nm and an extinction coefficient of 0.037 mg of oligo/mL. In all studies, six rats received 1.0 mg of oligonucleotide/kg of animal weight by bolus tail vein injection and EDTA plasma samples were taken at various times from 2 min to 4 h. The standards, plasma samples, and quality control samples were analyzed using a hybridization assay. The hybridization assay utilized a capture oligonucleotide that contains a complementary sequence at the 5′ end of the VEGF aptamer conjugated to an iron oxide (FeO) bead [FeO-spacer-3′-d(GCCTTAGTCACTT)-5′ where spacer = $(dT)_8$] and a detection oligonucleotide containing two biotin molecules at the 5′ end [biotin-biotin-5′-d(spacer-CGGATGTATAAG-

CA)-3′, where spacer = $(dT)_8$]. After incubation of the capture and detection probes with a plasma sample containing VEGF aptamers, the amount of the biotin oligonucleotide hybridized to the bead was quantitated with the strepavidin-linked alkaline phosphatase, using CSPD-Sapphire (Tropix, Bedford, MA) as the luminescent substrate. For each aptamer, the standard curve and quality control samples were matched to the aptamer being analyzed. Standard curves were fit using a four-parameter logistic equation (PRISM, version 2.00, GraphPad, San Diego, CA). Sample and quality control concentrations were extrapolated from the standard curve and corrected for dilution. Data for each formulation were pooled, and the pharmacokinetic parameters were analyzed using two-compartment compartmental analysis (weighting $1/y^2$, WinNonlin Pro, version 1.1.12, Scientific Consulting, Inc., Apex, NC).

Competition Electrophoretic Mobility Shift Assay. ^{32}P 5′ end-labeled NX213 (1.5 nM) was incubated in binding buffer (phosphate-buffered saline with 0.01% human serum albumin) at 37 °C for 20 min in the presence of VEGF-165 (R&D Systems, Minneapolis, MN; 0.33 nM) and competitor oligonucleotide (5 pM to 0.33 μM). The [^{32}P]NX213−VEGF complex was resolved from the free [^{32}P]NX213 by electrophoresis on an 8% polyacrylamide gel (19:1 acrylamide/bisacrylamide, Tris-borate, 89 mM, and 1 mM EDTA as the running buffer). The intensity of the band corresponding to the [^{32}P]-NX213−VEGF complex at varying competitor concentrations was quantitated by phosphorimager analysis. Data normalized for the amount of complex formed in the absence of competitor were fitted by the least-squares method to a competition binding equation that describes the mutually exculsive binding of two species to the same target (*28*).

Receptor Binding Inhibition. Confluent cultures of HUVECs in 24-well plates were incubated with [^{125}I]-VEGF-165 (Amersham, Arlington Heights, IL; 20 ng/mL) and varying amounts of aptamers for 2 h at 4 °C. At the end of the 2 h incubation period, the supernatant was aspirated and the wells were washed two times with cold PBS. HUVECs were then lysed with 1% Triton X-100, and the amount of cell-associated [^{125}I]VEGF was determined by γ counting.

[^3H]Thymidine Incorporation Assay. HUVECs (population doubling of 4−12) were plated at a density of 10^4/well on 96-well plates in MEM supplemented with 10 mM HEPES (pH 7.4) and 1 μg/mL heparin (from porcine lungs, Sigma, St. Louis, MO). Following a 4−5 h attachment period, quiescence was induced by overnight incubation in MEM containing 0.5% fetal bovine serum and 1 μg/mL heparin. VEGF was then added to the cell cultures in the presence or absence of aptamers for a period of 48 h. [^3H]Thymidine was added in the last 24 h of incubation, and the amount of DNA-associated [^3H]thymidine was determined by scintillation counting.

Dermal Vascular Permeability Assay. The ability of the test aptamers to attenuate VEGF-induced changes in the permeability of the dermal vasculature (Miles assay) was performed as previously described (*15*, *29*) with minor modifications. Briefly, adult female guinea pigs (three per study) were anesthetized with isoflurane, and the hair on the dorsal and lateral back areas was removed with clippers. Evans Blue dye (2.5 mg/guinea pig) was administered intravenously. Injection solutions (PBS, VEGF, and aptamers) were prepared ≥30 min in advance and comixed where indicated. Each solution shown was then injected intradermally (duplicate injections for each guinea pig, 40 μL/site) in a randomized manner in a grid pattern drawn on the clippered area. Guinea pigs were allowed to recover from anesthesia and were sacrificed by CO_2 exposure 30 min after completion of the intradermal injections. The skin was harvested, trimmed free of subcutis, and transilluminated. Images were then captured using a color CCD camera (Hitachi Denshi KP-50U) and Image-Pro Plus software (version 3.1, Media Cybernetics, Silver Springs, MD). Each skin sample was normalized for intensity with each injection site analyzed for optical density and the area involved.

Chicken Allantoic Membrane (CAM) Assay. The effect of various VEGF aptamers on VEGF-induced angiogenesis was tested in CAMs. Angiogenesis was induced in CAMs by placing filter disks saturated with VEGF on 10-day-old embryos. Coded test compounds (1 μM) or an equal amount of the carrier buffer (100 μL) was injected into the vessels on the following day. CAMs were resected on day 3 and analyzed using an Olympus stereomicroscope. The number of branching blood vessels infiltrating under the disk were counted and photographed. The average number of blood vessels under the disks soaked in buffer alone were subtracted from all groups.

RESULTS

Preparation of Liposome-Anchored VEGF Aptamers. To allow stable membrane anchoring, we used the solid phase phosphoramidite method to prepare a lipid derivative of the VEGF aptamer in which two 18-carbon saturated unbranched hydrocarbon chains were attached via glycerol ether linkages. The dialkylglycerol (DAG) phosphoramidite containing a tetraethylene glycol spacer was synthesized in seven steps and introduced at the 5′ end of the VEGF aptamer (Figure 1A,B). DAG−NX213 was readily purified by reverse phase HPLC since the retention time of the lipid-containing aptamer is considerably greater than that of the aptamer without the lipid group. To incorporate DAG−NX213 into the bilayer of liposomes, we sonicated a solution of DAG−NX213 (1 mg/mL) in 25 mM sodium phosphate buffer (pH 7.4) containing 9% sucrose in the presence of a 50 mg/mL spray-dried hydrated mixture of distearoylphosphatidylcholine (DSPC) and cholesterol (2 mol:1 mol). The ratio of DAG−NX213 to lipids was chosen arbitrarily and is not optimized for any purpose. On the basis of size exclusion chromatography, all of the DAG−aptamer was found to be associated with the liposome fraction following sonication. Importantly, aptamer fragments were not observed following liposome preparation, either by size exclusion chromatography or by HPLC, indicating that the DAG−aptamer is stable to sonication conditions (data not shown). In a typical preparation, liposomes with a mean diameter of ≈50−65 nm were obtained (Figure 2A). Liposomes prepared in this manner were visualized by electron microscopy in freeze-fracture preparations (*30*) (Figure 2B). Assuming surface areas of 44.5 Å for DSPC and 39 Å for cholesterol (*31*), for spherical liposomes with a homogeneous lipid distribution [2 mol of DSPC (MW = 790.2) per mole of cholesterol (MW = 386.7)] and a membrane thickness of 50 Å, we calculated the number of lipids per liposome to be 3.02×10^4 and 4.88×10^4 for liposomes with 50 and 65 nm diameters, respectively. On the basis of these values, we estimate that there are on average approximately 34−60 aptamers per liposome for 50−65 nm liposomes.

In the absence of the DAG−NX213 aptamer, liposomes with a comparable size distribution were obtained using

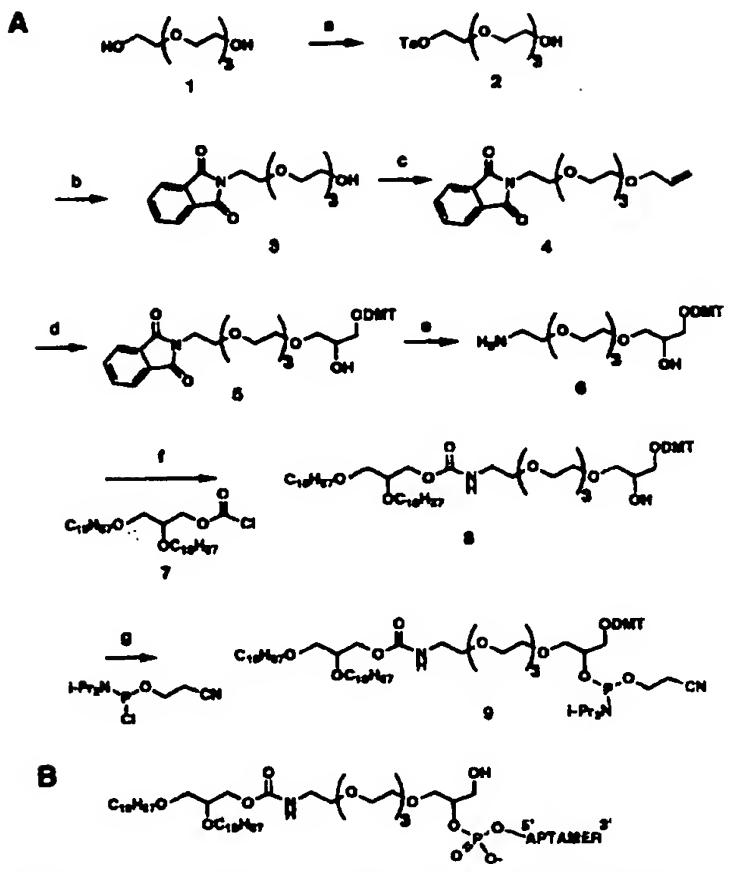

Figure 1. Synthesis of the DAG-modified VEGF aptamer. (A) DAG phosphoramidite was synthesized in eight steps using the following reagents and conditions: (a) 0.1 equiv of toluenesulfonyl chloride, pyridine (75%); (b) phthalimide, 1,8-diazabicyclo-[5.4.0]undec-7-ene, dimethylformamide, 80 °C (80%); (c) allyl bromide, NaH, tetrahydrofuran (67%); (d) step 1, 0.5 equiv of OsO_4, 1.05 equiv of *N*-methylmorpholine *N*-oxide, acetone/water (99:1); step 2, dimethoxytrityl (DMT) chloride, pyridine (89% for two steps); (e) 40% methylamine (95%); (f) 1,2-di-*O*-octadecyl-*sn*-glycerol chloroformate (**7**), pyridine (57%); (g) 2 equiv of diisopropylethylamine, methylene chloride (95%). The synthesis is further described in Experimental Procedures. (B) Structure of the DAG-aptamer.

the same lipid composition and method of liposome preparation (data not shown). To determine the partitioning of the aptamers between the inside and outside surfaces of liposomes, we examined the accessibility of DAG–NX213 in the liposomal formulation (DAG–NX213-L) to ribonuclease T_1 (Figure 2C). With two riboguanosines in the sequence (*9*), DAG–NX213 is efficiently cleaved by ribonuclease T_1 (Figure 2C, lanes 3 and 4). Simple incubation of DAG–NX213 with preformed liposomes does not protect the aptamer from ribonuclease T_1 (Figure 2C, lanes 5 and 6). However, when DAG–NX213 is incorporated in liposomes by sonication (DAG–NX213-L), about one-third is protected from the nuclease (Figure 2C, lane 11). The addition of 0.1% Triton X-100 to DAG–NX213-L, which disrupts the liposomes without affecting the activity of the nuclease (compare lanes 3 and 4 or 7 and 8 in Figure 2C), exposes the previously protected aptamer to digestion (Figure 2C, lane 12). These results are consistent with the notion that the aptamer is distributed on both sides of the bilayer (Figure 2D).

Plasma Pharmacokinetic Properties of Free, Lipid-Modified, and Liposomal VEGF Aptamers (NX213, DAG–NX213, and DAG–NX213-L). The concentrations of NX213, DAG–NX213, and DAG–NX213-L in plasma of Sprague-Dawley rats as a function of time are shown in Figure 3, and the parameters from compartmental analysis (see Experimental Procedures) are summarized in Table 1. The majority of NX213 is cleared rapidly in the α phase with a $t_{1/2}$ of 7 min and an overall clearance rate of 6.8 mL kg^{-1} min^{-1}. Conjugation of the DAG group to the aptamer results in highly biphasic clearance from plasma with an increased $\beta(t_{1/2})$ and a somewhat slower overall rate of clearance (4.95 mL kg^{-1} min^{-1}) relative to those of NX213. Incorporation of DAG–NX213 into liposomes shows a substantial additional decrease in clearance of the aptamer from plasma (1.88 mL kg^{-1} min^{-1}).

Binding of VEGF Aptamers to VEGF. We next examined the binding affinities of NX213, DAG–NX213, and DAG–NX213-L for VEGF using a competition electrophoretic mobility shift method (Figure 4 and Table 2). The binding affinity of DAG–NX213 for VEGF was comparable to that of NX213. The apparent binding affinity of DAG–NX213-L was ≈3-fold lower than that of DAG–NX213. A part of the observed affinity reduction is probably due to the confinement of a fraction of the aptamer population to the liposome interior. In any event, most of the binding affinity of the aptamer is clearly retained in the liposomal formulation. For comparison, compositionally identical analogues of these aptamers in which the sequence that defines high-affinity binding was arbitrarily scrambled (scNX213 = 5′-dT^{s}dT^{s}dT^{s}dT^{s}mGaUaCmGmGaUmAaCrGmGrAmGaUmGrGrAaCaCmGaUaCmAaCmGdT^{s}dT^{s}dT^{s}dT^{s}dT-3′) bind to VEGF with substantially lower affinities (Figure 4 and Table 2).

Effect of VEGF Aptamers on Binding of VEGF to Cell Surface Receptors. Cellular responses to VEGF are initiated by binding of the growth factor to its cell surface receptors. We have tested the VEGF aptamers for their ability to inhibit the binding of [^{125}I]VEGF to receptors expressed on human umbilical vein endothelial cells (HUVECs) (Figure 5). As previously observed, the free aptamer (NX213) inhibited receptor binding in a concentration-dependent manner with an EC_{50} of ≈1 nM. In comparison, DAG–NX213 and DAG–NX213-L inhibited receptor binding with ≈5-fold lower potency. The sequence-scrambled analogues of these aptamers up to 1 μM were unable to inhibit receptor binding.

Effect of VEGF Aptamers on VEGF-Induced Endothelial Cell Proliferation. The effect of various VEGF aptamers on VEGF-induced endothelial cell proliferation was examined by measuring the amount of [^{3}H]-thymidine uptake in HUVECs (Figure 6). Maximal stimulation of [^{3}H]thymidine uptake in a 3 day proliferation assay was observed with VEGF concentrations of >1 ng/mL (Figure 6A). In contrast to its very potent inhibition of VEGF receptor binding, NX213 up to 1 μM was unable to inhibit HUVEC proliferation induced with 3 ng/mL VEGF (Figure 6B). Under the same conditions, DAG–NX213 and DAG–NX213-L, on the other hand, inhibited the VEGF-induced HUVEC proliferation in a dose-dependent manner with similar EC_{50} values of ≈3 nM. The sequence-scrambled analogues of DAG–NX213 and DAG–NX213-L were inhibitory only at concentrations greater than ≈300 nM.

Effect of VEGF Aptamers on VEGF-Induced Capillary Permeability Increases. VEGF is the only known angiogenic growth factor that transiently enhances capillary permeability to macromolecules. In response to VEGF, an increase in vascular permeability causes extravasation of albumin-bound Evans blue dye, resulting in a blue spot at the site of injection (Miles assay) (*15*, *29*). The inhibitory effect of the VEGF aptamers on the VEGF-induced capillary permeability

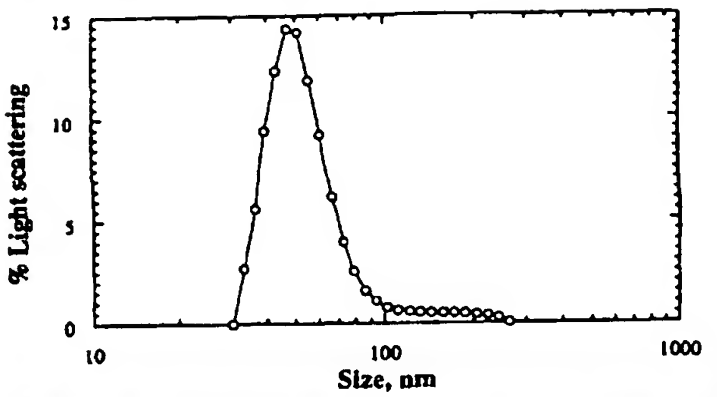

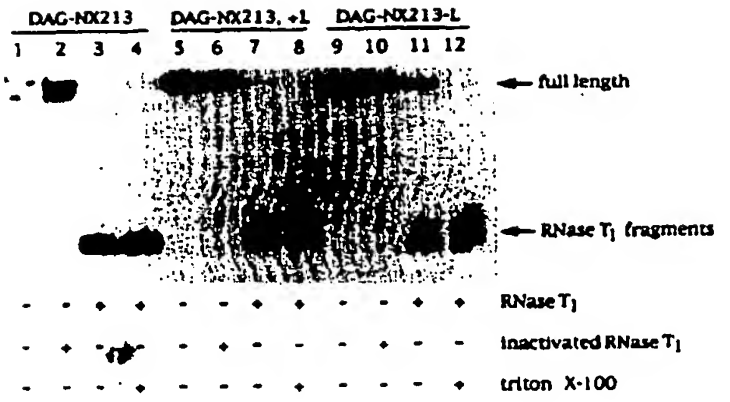

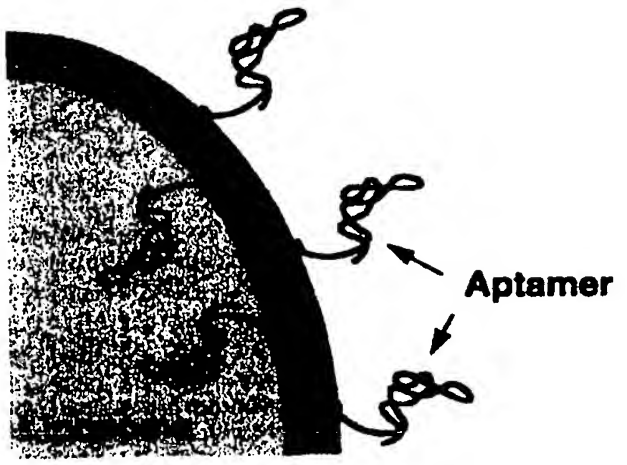

Figure 2. Characterization of physical properties of the liposomal VEGF aptamer (DAG−NX213-L). (A, top left) The size of DAG−NX213-L particles was determined by quasi-elastic light scattering using a Leeds & Northrup Model Microtrack UPA 150 particle analyzer (Horsham, PA). The distribution by liposome volume as a function of diameter is shown. (B, bottom left) Freeze-fracture electron micrograph of DAG−NX213-L. (C, top right) Accessibility of DAG−NX213 to ribonuclease T_1 as a function of formulation. RNase T_1 digests of DAG−NX213 alone (lanes 1−4), DAG−NX213 mixed with preformed liposomes (lanes 5−8), and DAG−NX213 incorporated into liposomes by sonication (DAG−NX213-L, lanes 9−12) are shown resolved on a 20% polyacrylamide/7 M urea gel. In the first lane of each set (lanes 1, 5, and 9), no RNase was added. In the second lane of each set (lanes 2, 6, and 10), the gel loading solution (which inactivates the RNase) was added to the samples prior to adding RNase. In the third lane of each set (lanes 3, 7, and 11), the samples were incubated with RNase T_1 for 30 min at 20 °C. In the fourth lane of each set (lanes 4, 8, and 12), the samples were incubated with RNase T_1 for 30 min at 20 °C in the presence of 0.1% Triton X-100. (D, bottom right) Schematic representation of liposome-anchored aptamers.

increase was studied in guinea pigs (Figure 7). Test aptamers at various concentrations were coinjected intradermally with VEGF (20 nM) in guinea pigs preinjected with Evans blue dye. Because the recovery of the dye by organic solvent extraction is generally very inefficient, we have developed a quantitation method that measures the absorption of light through the skin. NX213 at concentrations up to 10 μM was not able to inhibit the vascular permeability activity of VEGF. DAG−NX213 and DAG−NX213-L, on the other hand, inhibited about 60 and 90% of the VEGF-induced permeability increase, respectively, at the highest aptamer concentration tested (10 μM), with comparable IC_{50} values of 0.3−0.5 μM. Sequence-scrambled analogues of these compounds were not inhibitory (data not shown).

Effect of VEGF Aptamers on VEGF-Induced Angiogenesis in Chicken Chorioallantoic Membranes (CAMs). VEGF is a potent inducer of angiogenesis in a number of in vivo model systems. The effect of various VEGF aptamers on VEGF-induced angiogenesis was tested in CAMs. Capillary vessel formation within the CAMs has been used extensively as a convenient in vivo model system for studying the angiogenic and angiostatic activity of various compounds (*32*). Angiogenesis was induced in CAMs by placing filter disks saturated with VEGF on 10-day-old embryos. Coded test compounds (1 μM) or an equal amount of the carrier buffer (100 μL) was injected into the vessels on the following day. CAMs were resected on day 3 and analyzed using a stereomicroscope. The number of branching blood vessels infil-

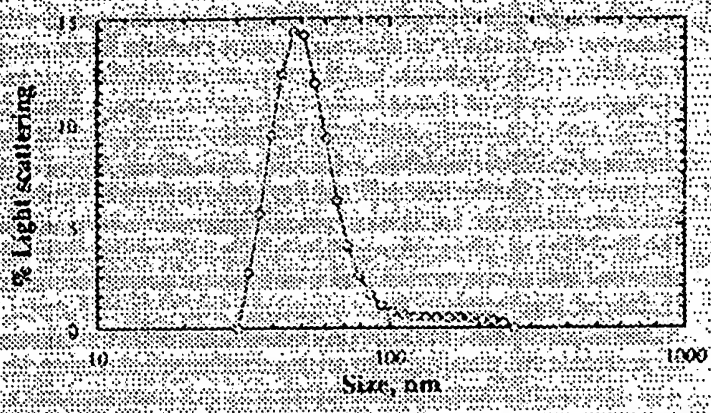

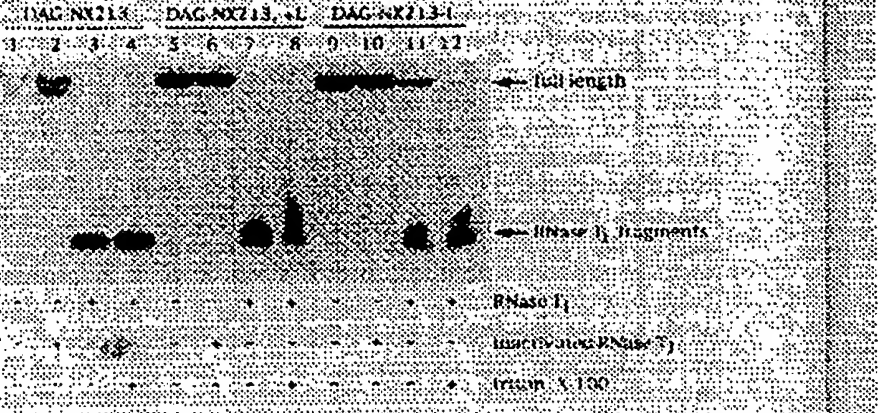

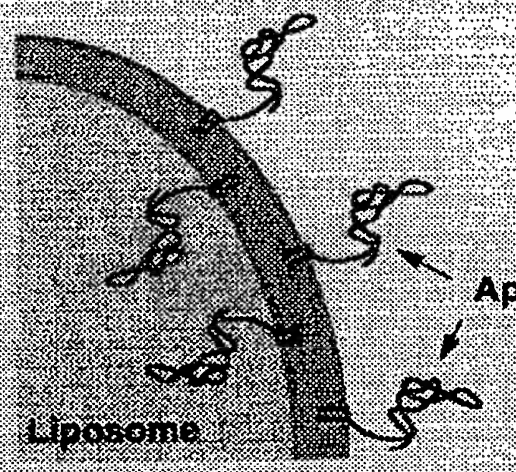

Figure 2. Characterization of physical properties of the liposomal VEGF aptamer (DAG–NX213-L). (A, top left) The size of DAG–NX213-L particles was determined by quasi-elastic light scattering using a Leeds & Northrup Model Microtrack UPA 150 particle analyzer (Horsham, PA). The distribution by liposome volume as a function of diameter is shown. (B, bottom left) Freeze-fracture electron micrograph of DAG–NX213-L. (C, top right) Accessibility of DAG–NX213 to ribonuclease T_1 as a function of formulation. RNase T_1 digests of DAG–NX213 alone (lanes 1–4), DAG–NX213 mixed with preformed liposomes (lanes 5–8), and DAG–NX213 incorporated into liposomes by sonication (DAG–NX213-L, lanes 9–12) are shown resolved on a 20% polyacrylamide/7 M urea gel. In the first lane of each set (lanes 1, 5, and 9), no RNase was added. In the second lane of each set (lanes 2, 6, and 10), the gel loading solution (which inactivates the RNase) was added to the samples prior to adding RNase. In the third lane of each set (lanes 3, 7, and 11), the samples were incubated with RNase T_1 for 30 min at 20 °C. In the fourth lane of each set (lanes 4, 8, and 12), the samples were incubated with RNase T_1 for 30 min at 20 °C in the presence of 0.1% Triton X-100. (D, bottom right) Schematic representation of liposome-anchored aptamers.

increase was studied in guinea pigs (Figure 7). Test aptamers at various concentrations were coinjected intradermally with VEGF (20 nM) in guinea pigs preinjected with Evans blue dye. Because the recovery of the dye by organic solvent extraction is generally very inefficient, we have developed a quantitation method that measures the absorption of light through the skin. NX213 at concentrations up to 10 μM was not able to inhibit the vascular permeability activity of VEGF. DAG–NX213 and DAG–NX213-L, on the other hand, inhibited about 60 and 90% of the VEGF-induced permeability increase, respectively, at the highest aptamer concentration tested (10 μM), with comparable IC_{50} values of 0.3–0.5 μM. Sequence-scrambled analogues of these compounds were not inhibitory (data not shown).

Effect of VEGF Aptamers on VEGF-Induced Angiogenesis in Chicken Chorioallantoic Membranes (CAMs). VEGF is a potent inducer of angiogenesis in a number of in vivo model systems. The effect of various VEGF aptamers on VEGF-induced angiogenesis was tested in CAMs. Capillary vessel formation within the CAMs has been used extensively as a convenient in vivo model system for studying the angiogenic and angiostatic activity of various compounds (32). Angiogenesis was induced in CAMs by placing filter disks saturated with VEGF on 10-day-old embryos. Coded test compounds (1 μM) or an equal amount of the carrier buffer (100 μL) was injected into the vessels on the following day. CAMs were resected on day 3 and analyzed using a stereomicroscope. The number of branching blood vessels infil-

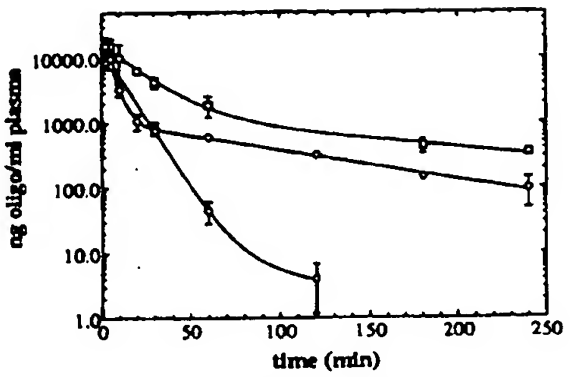

Figure 3. Plasma pharmacokinetic properties of NX213, DAG–NX213, and DAG–NX213-L in Sprague-Dawley rats. Aptamers were administered by intravenous injection via the tail vein, at a dose of 1 mg of aptamer per kilogram of animal weight. EDTA plasma samples were analyzed using a double-hybridization assay: NX213 (○), DAG–NX213 (◇), and DAG–NX213-L (□). Data from two to five animals were used per data point (±SEM).

Table 1. Summary of Aptamer Pharmacokinetic Parameters in Plasma after Intravenous Bolus Administration in Sprague-Dawley Rats Determined from the Data Shown in Figure 3 (Compartmental Analysis)

parameter	NX213	DAG–NX213	DAG–NX213-L
total AUC (μg min^{-1} mL^{-1})[a]	147	202	531
C, t = 0 min (μg/mL)	14.59	23.16	16.95
C, t = 2 min (μg/mL)	15.31	14.08	15.74
$\alpha(t_{1/2})$ (min)	7	3	13
$\beta(t_{1/2})$ (min)	49	67	113
clearance (mL kg^{-1} min^{-1})	6.80	4.95	1.88
V_{ss} (mL/kg)	72	251	152

[a] AUC = area under the curve.

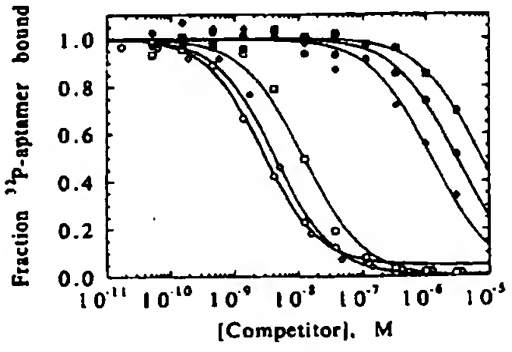

Figure 4. Binding affinities of NX213, DAG–NX213, and DAG–NX213-L and their sequence-scrambled analogues for VEGF. A competition electrophoretic mobility shift assay was used to determine the binding affinities of NX213 (○), DAG–NX213 (◇), and DAG–NX213-L (□) and their sequence-scrambled analogues scNX213 (●), DAG–scNX213 (◆), and DAG–scNX213-L (■). In all cases, competitor concentration refers to the total concentration of oligonucleotide (without a correction for aptamer accessibility).

trating under the disk were counted and photographed. The average number of blood vessels under the disks soaked in buffer alone was subtracted from all groups. The only compound that effectively blocked VEGF-induced angiogenesis was DAG–NX213-L, while NX213, DAG–NX213, and DAG–scNX213-L had a smaller effect or no effect (Figure 8).

DISCUSSION

The SELEX process has recently emerged as an efficient method of identifying aptamers with high affinities

Table 2. Relative Binding Affinities of NX213, DAG–NX213, DAG–NX213-L, and Their Sequence-Scrambled Analogues[a]

aptamer	$K_d^{aptamer}/K_d^{NX213}$ [a]
NX213	(1.0)
DAG–NX213	1.6 ± 0.3
DAG–NX213-L	4.7 ± 0.7
scNX213	(1.3 ± 0.9) × 10^3
DAG–scNX213	(5.0 ± 0.7) × 10^2
DAG–scNX213-L	(3.1 ± 3.4) × 10^3

[a] The value of K_d for NX213 binding to VEGF calculated from the competition binding experiment is (3.2 ± 0.2) × 10^{-10} M.

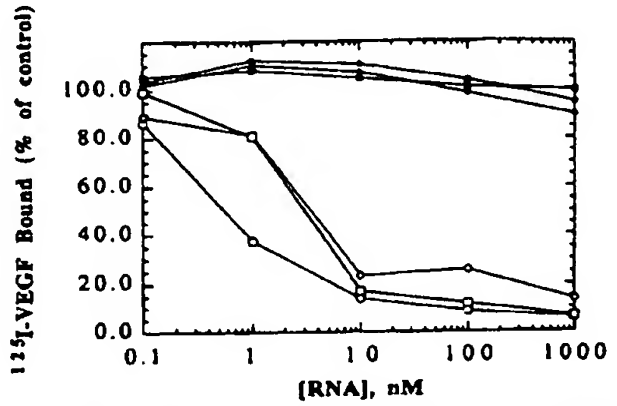

Figure 5. Effect of NX213, DAG–NX213, and DAG–NX213-L aptamers and their sequence-scrambled analogues on the binding of [^{125}I]VEGF to cell surface receptors expressed on human umbilical vein endothelial cells (HUVECs). Confluent cultures of HUVECs were incubated with 20 ng/mL [^{125}I]VEGF and varying amounts of NX213 (○), DAG–NX213 (◇), and DAG–NX213-L (□) and their sequence-scrambled analogues scNX213 (●), DAG–scNX213 (◆), and DAG–scNX213-L (■). Data points represent averages of two determinations.

for a variety of molecular targets. As chemically synthesized molecules, aptamers are uniquely amenable to a wide range of chemical modifications. In attempts to develop aptamer-based drug candidates, many such modifications have been aimed at improving the functional efficacy of the aptamers in vivo. For example, the affinity, specificity, and nuclease resistance have been substantially improved by the introduction of a series of 2′-*O*-methylpurine substitutions (*9*). Hicke et al. have recently shown that poly(ethylene glycol)-derivatized L-selectin DNA aptamers have improved pharmacokinetic properties and that this translated into more effective inhibition of lymphocyte trafficking in vivo (*33*).

Here we have shown that a lipid group such as DAG can be introduced into a prototypic aptamer with minimal effects on the binding affinity. Although we have employed the solid phase phosphoramidite method to conjugate the DAG group to the aptamer, solution coupling methods as well as other types of coupling chemistries are clearly feasible. Indeed, it has been demonstrated previously that hydrophobic groups can be introduced into oligonucleotides by a variety of methods and that such lipid–oligonucleotide conjugates have altered physical and pharmacokinetic properties (*34*–*38*). Lipid groups such as DAG permit stable anchoring into bilayers of liposomes. This notion has been recognized previously and exploited for improving the circulating levels in plasma of low-molecular weight molecules such as small peptides and carbohydrates (*39*, *40*).

The plasma circulating time of the lipid-modified VEGF aptamer (DAG–NX213) is somewhat improved compared to that of the underivatized aptamer (NX213),

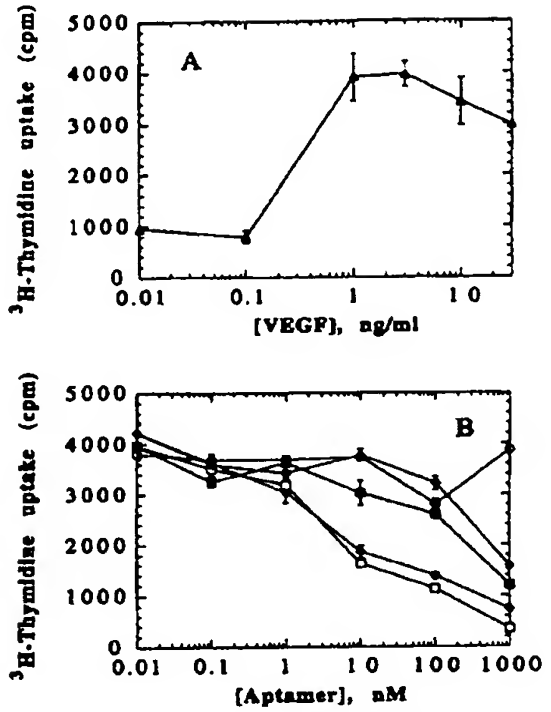

Figure 6. Effect of NX213, DAG–NX213, and DAG–NX213-L aptamers and their sequence-scrambled analogues on VEGF-induced HUVEC proliferation. (A) Dose response of VEGF added to the culture medium. (B) The effect of NX213 (○), DAG–NX213 (◇), DAG–NX213-L (□), DAG–scNX213 (◆), and DAG–scNX213-L (■) on HUVEC proliferation induced with 3 ng/mL VEGF. Values are the mean (five determinations) ± SEM.

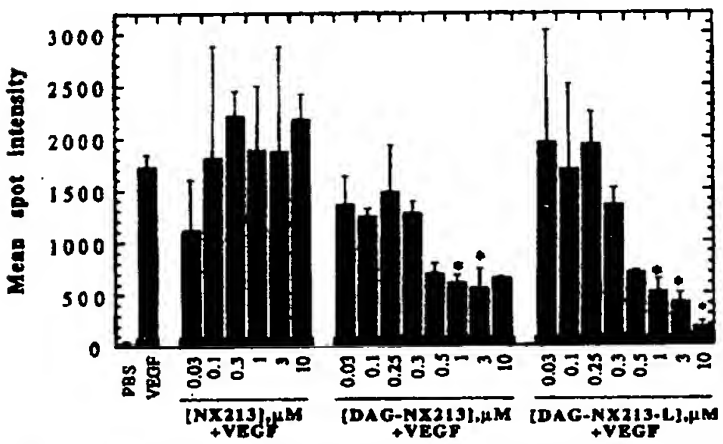

Figure 7. Effect of NX213, DAG–NX213, and DAG–NX213-L aptamers on VEGF-induced vascular permeability increase. The local extravasation of Evans blue dye was determined 30 min after injection of VEGF (0.8 pmol) in the presence or absence of aptamers by transillumination of harvested skin. Values are the mean (two to ten determinations) ± SEM. An asterisk indicates that $P < 0.05$ compared with that for VEGF alone.

as has been observed with other lipid-modified nucleic acids (*38*). This is probably the result of the association of DAG–NX213 with lipoproteins in plasma (*38*). Liposome anchoring of the DAG–NX213 aptamer, however, clearly leads to a further substantial increase in its plasma lifetime. Liposomes with the same lipid composition and size as those used in this work in which the unconjugated aptamer (NX213) was encapsulated in the interior of the liposome exhibit considerably longer plasma residence times (total AUC ≈ 4900 μg min^{-1} mL^{-1}, clearance ≈ 0.2 mL kg^{-1} min^{-1}; see Table 1) compared with liposomes that carry DAG–NX213 in their bilayers (data not shown). Thus, like peptides and

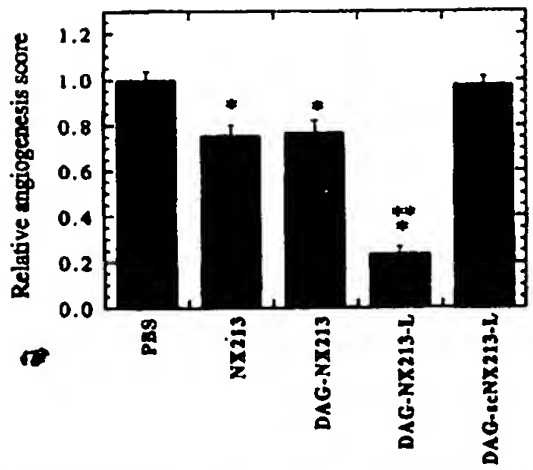

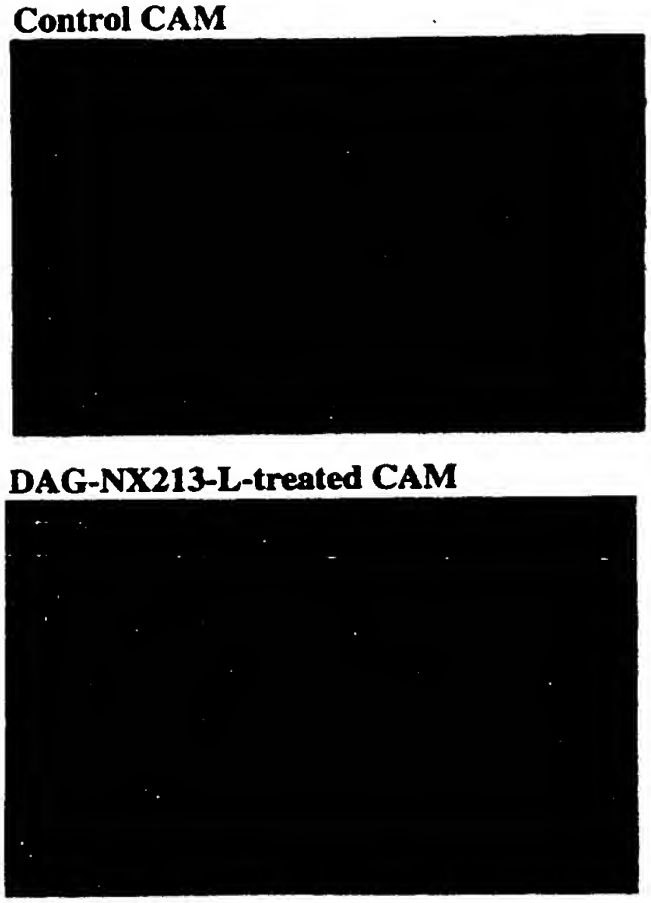

Figure 8. Effect of NX213, DAG–NX213, and DAG–NX213-L aptamers and their sequence-scrambled analogues on VEGF-induced angiogenesis in CAMs. VEGF-saturated filter disks were used on 10-day-old CAMs to induce angiogenesis. Test compounds or buffer (PBS) was injected intravascularly on the following day, and the number of branching blood vessels infiltrating the disks were counted on day 3. Five to twelve CAMs were studied for each compound, and the experiments were repeated at least two times with similar results. (A, top) Relative angiogenesis scores normalized to the number of new blood vessels observed in the group of CAMs containing the VEGF-saturated disks and treated with PBS alone (±SEM). An asterisk indicates that $P < 0.05$ compared with that of the control (PBS) group alone, and two asterisks indicate that $P < 0.05$ compared with that of NX213 or DAG–NX213. (B, bottom) Representative CAMs containing VEGF-saturated disks (covering the entire CAM) treated with buffer alone (upper panel) or DAG–NX213-L (lower panel).

antibodies (*39*, *41*), surface-immobilized aptamers appear to reduce the plasma residence times of liposomes.

Liposome anchoring of DAG–NX213 causes a small apparent reduction in the binding affinity for VEGF (Figure 4) which is probably due in part to the fact that

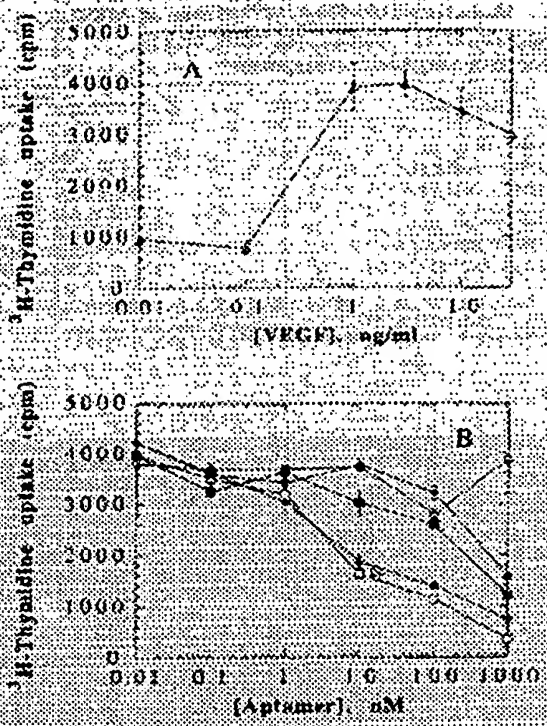

Figure 6. Effect of NX213, DAG–NX213, and DAG–NX212-L aptamers and their sequence-scrambled analogues on VEGF-induced HUVEC proliferation. (A) Dose response of VEGF added to the culture medium. (B) The effect of NX213 (○), DAG–NX213 (◇), DAG–NX212-L (□), DAG–scNX213 (◆), and DAG–scNX213-L (■) on HUVEC proliferation induced with 3 ng/mL VEGF. Values are the mean (five determinations) ± SEM.

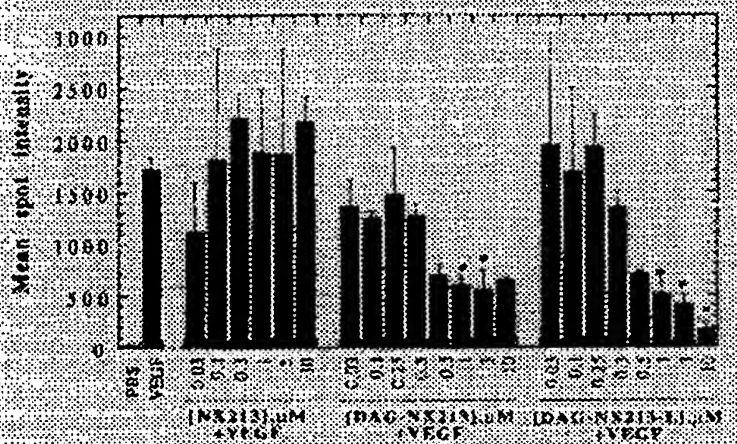

Figure 7. Effect of NX213, DAG–NX213, and DAG–NX213-L aptamers on VEGF-induced vascular permeability increase. The local extravasation of Evans blue dye was determined 30 min after injection of VEGF (0.5 pmol) in the presence or absence of aptamers by transillumination of harvested skin. Values are the mean (two to ten determinations) ± SEM. An asterisk indicates that $P < 0.05$ compared with that for VEGF alone.

as has been observed with other lipid-modified nucleic acids (*38*). This is probably the result of the association of DAG–NX213 with lipoproteins in plasma (*38*). Liposome anchoring of the DAG–NX213 aptamer, however, clearly leads to a further substantial increase in its plasma lifetime. Liposomes with the same lipid composition and size as those used in this work in which the unconjugated aptamer (NX213) was encapsulated in the interior of the liposome exhibit considerably longer plasma residence times (total AUC ≈ 4900 μg min^{-1} mL^{-1}, clearance ≈ 0.2 mL kg^{-1} min^{-1}; see Table 1) compared with liposomes that carry DAG–NX213 in their bilayers (data not shown). Thus, like peptides and

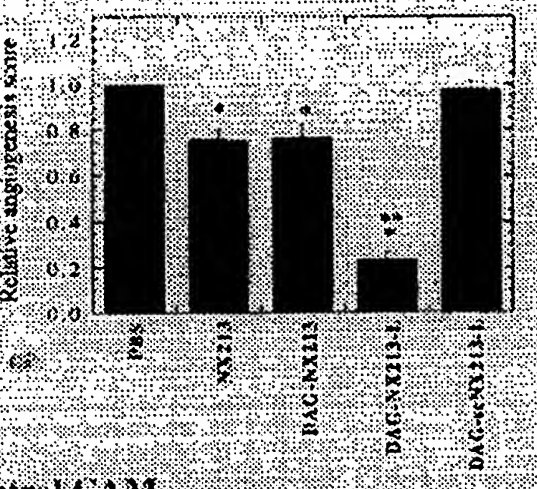

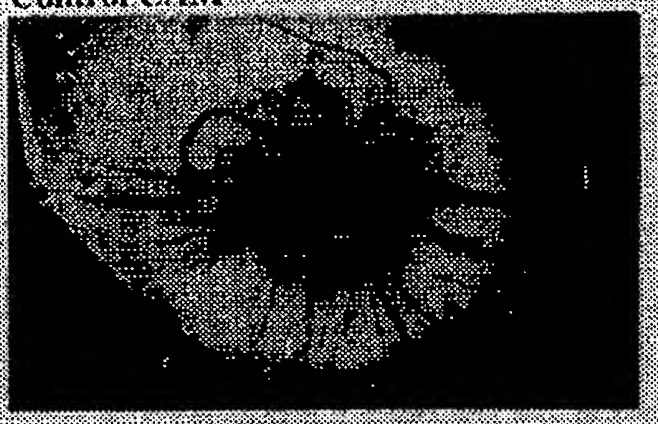

Figure 8. Effect of NX213, DAG–NX213, and DAG–NX213-L aptamers and their sequence-scrambled analogues on VEGF-induced angiogenesis in CAMs. VEGF-saturated filter disks were used on 10-day-old CAMs to induce angiogenesis. Test compounds or buffer (PBS) was injected intravascularly on the following day, and the number of branching blood vessels infiltrating the disks were counted on day 3. Five to twelve CAMs were studied for each compound, and the experiments were repeated at least two times with similar results. (A, top) Relative angiogenesis scores normalized to the number of new blood vessels observed in the group of CAMs containing the VEGF-saturated disks and treated with PBS alone (±SEM). An asterisk indicates that $P < 0.05$ compared with that of the control (PBS) group alone, and two asterisks indicate that $P < 0.05$ compared with that of NX213 or DAG–NX213. (B, bottom) Representative CAMs containing VEGF-saturated disks (covering the entire CAM) treated with buffer alone (upper panel) or DAG–NX213-L (lower panel).

antibodies (*39*, *41*), surface-immobilized aptamers appear to reduce the plasma residence times of liposomes.

Liposome anchoring of DAG–NX213 causes a small apparent reduction in the binding affinity for VEGF (Figure 4) which is probably due in part to the fact that

some of the aptamer is anchored in the inner leaflet of the bilayer and is therefore inaccessible to VEGF in solution. However, since liposome anchoring also creates a multivalent display of the aptamer (which is expected to increase the apparent affinity) in addition to imposing steric and orientational contraints on binding (which may reduce the apparent affinity), a straightforward interpretation of affinity is not possible from the data. Like NX213, DAG–NX213 and DAG–NX213-L aptamers inhibited the binding of VEGF to its endothelial cell receptors, albeit at ≈5-fold reduced potency compared with that of NX213. In contrast to the modest reduction in the binding affinity for VEGF and in the receptor binding inhibitory activity, DAG–NX213 and DAG–NX213-L exhibited a considerably greater potency in inhibiting VEGF-induced DNA synthesis in endothelial cells compared with NX213 (NX213 showed no inhibition up to 1 μM). Similar inhibitory activity enhancement was observed with DAG–NX213 and DAG–NX213-L compared to that with NX213 in the vascular permeability assay, with DAG–NX213-L showing the most complete inhibition and NX213 being ineffective up to 10 μM. In the CAM angiogenesis assay, DAG–NX213-L was the only aptamer that showed effective inhibition of VEGF-induced angiogenesis.

The reason for the inhibitory activity enhancement of DAG–NX213 and DAG–NX213-L in vitro and in vivo remains to be elucidated. It will be important to establish whether DAG–NX213 and DAG–NX213-L (or similar preparations) associate with cellular plasma membranes in the mitogenicity assay and whether the larger size of these aptamers (especially of the liposomal aptamer) results in slower diffusion and therefore greater concentraion at the site of injection in the Miles assay. In the mitogenicity and Miles assays, since VEGF is administered along with the aptamers in a confined space, the longer plasma circulating times of DAG–NX213 and DAG–NX213-L compared with that of NX213 are obviously not relevant. However, this may be important in the CAM assay where the aptamers were administered intravenously.

The association of aptamers with liposomes in a manner described here may have several applications of general utility. The advantages of such fomulations include (i) improving the plasma pharmacokinetics of aptamers, (ii) presenting aptamers in a multivalent array with the aim of increasing the avidity of interaction with their targets, (iii) combining two or more aptamers with different specificities in the same liposome particle, (iv) enhancing the delivery of aptamers to tumors by taking advantage of the intrinsic tumor targeting properties of liposomes, and (v) using the high affinity and specificity of aptamers to guide liposomal contents to specific targets, which has to date primarily been accomplished with antibodies (*41–43*). Aptamers are well-suited for the kinds of preparations described here since, unlike most proteins, the denaturation of aptamers by heat, various molecular denaturants, and organic solvents is readily reversible. Given the rapidly increasing availability of aptamers with different specificities, similar liposome-anchored aptamers to the ones described here will be tested soon.

ACKNOWLEDGMENT

We thank Drs. Paul Schmidt, Eric Forssen, and Gary Fujii for many useful discussions. We also thank Jeffrey Walenta, Joelle Brown, and Sarah O'Rourke for expert technical assistance, Chandra Vargeese and Philippe Bridonneau for assistance with large-scale oligonucleotide synthesis and purification, Julie Wolf for performing statistical analyses, and David Tinnermeier for performing electrospray mass spectroscopy analyses.

LITERATURE CITED

(1) Tuerk, C., and Gold, L. (1990) Systematic evolution of ligands by exponential enrichment: RNA ligands to bacteriophage T4 DNA polymerase. *Science 249*, 505–510.
(2) Ellington, A., and Szostak, J. (1990) In vitro selection of RNA molecules that bind specific ligands. *Nature 346*, 818–822.
(3) Gold, L. (1995) Oligonucleotides as research, diagnostic, and therapeutic agents. *J. Biol. Chem. 270*, 13581–13584.
(4) Gold, L., Polisky, B., Uhlenbeck, O. C., and Yarus, M. (1995) Diversity of oligonucleotide functions. *Annu. Rev. Biochem. 64*, 763–797.
(5) Lin, Y., Qiu, Q., Gill, S. C., and Jayasena, S. (1994) Modified RNA sequence pools for in vitro selection. *Nucleic Acids Res. 22*, 5229–5234.
(6) Latham, J. A., Johnson, R., and Toole, J. J. (1994) The application of a modified nucleotide in aptamer selection: novel thrombin aptamers containing 5-(1-pentynyl)-2′-deoxyuridine. *Nucleic Acids Res. 22*, 2817–2822.
(7) Jellinek, D., Green, L. S., Bell, C., Lynott, C. K., Gill, N., Vargeese, C., Kirschenheuter, G., McGee, D. P. C., Abesinghe, P., Pieken, W. A., Shapiro, R., Rifkin, D. B., Moscatelli, D., and Janjić, N. (1995) Potent 2′-amino-2′-deoxypyrimidine RNA inhibitors of basic fibroblast growth factor. *Biochemistry 34*, 11363–11372.
(8) Pagratis, N. C., Bell, C., Chang, Y.-F., Jennings, S., Fitzwater, T., Jellinek, D., and Dang, C. (1997) Potent 2′-amino- and 2′-fluoro-2′-deoxyribonucleotide RNA inhibitors of keratinocyte growth factor. *Nat. Biotechnol. 15*, 68–73.
(9) Green, L. S., Jellinek, D., Bell, C., Beebe, L. A., Feistner, B. D., Gill, S. C., Jucker, F. M., and Janjić, N. (1995) Nuclease-resistant nucleic acid ligands to vascular permeability factor/vascular endothelial growth factor. *Chem. Biol. 2*, 683–695.
(10) Folkman, J. (1995) Angiogenesis in cancer, vascular and other diesease. *Nat. Med. 1*, 27–31.
(11) Conn, G., Soderman, D. D., Schaeffer, M.-T., Wile, M., Hatcher, V. B., and Thomas, K. A. (1990) Purification of a glycoprotein vascular endothelial cell mitogen from a rat glioma-derived cell line (GS-9L). *Proc. Natl. Acad. Sci. U.S.A. 87*, 1323–1327.
(12) Gospodarowicz, D., Abraham, J. A., and Schilling, J. (1989) Isolation and characterization of a vascular endothelial cell mitogen produced by pituitary-derived folliculo stellate cells. *Proc. Natl. Acad. Sci. U.S.A. 86*, 7311–7315.
(13) Ferrara, N., and Henzel, W. J. (1989) Pituitary follicular cells secrete a novel heparin-binding growth factor specific for vascular endothelial cells. *Biochem. Biophys. Res. Commun. 161*, 851–858.
(14) Dvorak, H. F., Orenstein, N. S., Carvalho, A. C., Churchill, W. H., Dvorak, A. M., Galli, S. J., Feder, J., Bitzer, A. M., Rypysc, J., and Giovinco, P. (1979) Induction of fibrin-gel investment: an early event in line 10 hepatocarcinoma growth mediated by tumor-secreted products. *J. Immunol. 122*, 166–174.
(15) Senger, D. R., Galli, S. J., Dvorak, A. M., Peruzzi, C. A., Harvey, V. S., and Dvorak, H. F. (1983) Tumor cells secrete a vascular permeability factor that promotes accumulation of ascites fluid. *Science 219*, 983–985.
(16) Senger, D. R., Peruzzi, C. A., Feder, J., and Dvorak, H. F. (1986) A highly conserved vascular permeability factor secreted by a variety of human and rodent tumor cell lines. *Cancer Res. 46*, 5629–5632.
(17) Dvorak, H. F., Brown, L. F., Detmar, M., and Dvorak, A. M. (1995) Vascular permeability factor/vascular endothelial growth factor, microvascular hyperpermeability, and angiogenesis. *Am. J. Pathol. 146*, 1029–1039.
(18) Shweiki, D., Itin, A., Soffer, D., and Keshet, E. (1992) Vascular endothelial growth factor induced by hypoxia may mediate hypoxia-initiated angiogenesis. *Nature 359*, 843–845.

(19) Levy, A. P., Levy, N. S., and Goldberg, M. A. (1996) Post-transcriptional regulation of vascular endothelial growth factor by hypoxia. *J. Biol. Chem. 271*, 2746−2753.
(20) Thomas, K. A. (1996) Vascular endothelial growth factor, a potent and selective angiogenic agent. *J. Biol. Chem. 271*, 603−606.
(21) Brown, L. F., Detmar, M., Claffey, K., Nagy, J. A., Feng, D., Dvorak, A. M., and Dvorak, H. F. (1997) Vascular permeability factor/vascular endothelial growth factor: a multifunctional angiogenic cytokine. In *Regulation of Angiogenesis* (I. D. Goldberg and E. M. Rosen, Eds.) pp 233−269, Birkhauser, Basel, Switzerland.
(22) Houck, K. A., Ferrara, N., Winer, J., Cachianes, G., Li, B., and Leung, D. W. (1991) The vascular endothelial growth factor family: identificaiton of a fourth species and characterization of alternative splicing of RNA. *Mol. Endocrinol. 5*, 1806−1814.
(23) Tischer, E., Mitchell, R., Hartman, T., Silva, M., Gospodarowicz, D., Fiddes, J. C., and Abraham, J. A. (1991) The human gene for vascular endothelial growth factor. Multiple protein forms are encoded through alternative exon splicing. *J. Biol. Chem. 266*, 11947−11954.
(24) Millauer, B., Wizigmann-Voos, S., Schnurch, H., Martinez, R., Moller, N. P. H., Risau, W., and Ullrich, A. (1993) High affinity vascular endothelial growth factor binding and developmental expression suggest flk-1 as a major regulator of vasculogenesis and angiogenesis. *Cell 72*, 835−846.
(25) Terman, B. I., Carrion, M. E., Kovacs, E., Rasmussen, B. A., Eddy, R. L., and Shows, T. B. (1991) Identification of a new endothelial cell growth factor receptor tyrosine kinase. *Oncogene 6*, 519−524.
(26) de Vries, C., Escobendo, J. A., Ueno, H., Houck, K., Ferrara, N., and Williams, L. T. (1992) The fms-like tyrosine kinase, a receptor for vascular endothelial growth factor. *Science 255*, 989−991.
(27) Mustonen, T., and Alitalo, K. (1995) Endothelial receptor tyrosine kinases involved in angiogenesis. *J. Cell Biol. 129*, 895−898.
(28) Gill, S. C., Weitzel, S. E., and von Hippel, P. H. (1991) E. coli Sigma70 and NusA proteins. Binding interactions with core RNA polymerase in solution and within the transcription complex. *J. Mol. Biol. 220*, 307−324.
(29) Miles, A. A., and Miles, E. M. (1952) Vascular reactions to histamine, histamine-liberator, and leukotaxine in the skin of guinea pigs. *J. Physiol. (London) 118*, 228−257.
(30) Hope, M. J., Wong, K. F., and Cullis, P. R. (1989) Freeze-fracture of lipids and model membrane systems. *J. Electron Microsc. Tech. 13*, 277−287.
(31) Jain, M. K., and Wagner, R. C. (1980) *Introduction to Biological Membranes*, p 63, Wiley, New York.
(32) Auerbach, R., Auerbach, W., and Polakowski, I. (1991) Assays for angiogenesis: a review. *Pharmacol. Ther. 51*, 1−11.
(33) Hicke, B. J., Watson, S. R., Koenig, A., Lynott, C. K., Bargatze, R. F., Chang, Y.-F., Ringquist, S., Moon-McDermott, L., Jennings, S., Fitzwater, T., Han, H.-L., Varki, N., Albinana, I., Willis, M. C., Varki, A., and Parma, D. (1996) DNA aptamers block L-selectin function in vivo. Inhibition of human lymphocyte trafficking in SCID mice. *J. Clin. Invest. 98*, 2688−2692.
(34) Letsinger, R. L., Zhang, G., Sun, D. K., Ikeuchi, T., and Sarin, P. S. (1989) Cholesteryl-conjugated oligonucleotides: synthesis, properties, and activity as inhibitors of replication of human immunodeficiency virus in cell culture. *Proc. Natl. Acad. Sci. U.S.A. 86*, 6553−6556.
(35) Saison-Behmoaras, T., Tocqué, B., Rey, I., Chassignol, M., Thuong, N. T., and Hélène, C. (1991) Short modified antisense oligonucleotides directed against Ha-ras point mutations induce selective cleavage of the mRNA and inhibit T24 cells proliferation. *EMBO J. 10*, 1111−1118.
(36) Shea, R. G., Marsters, J. C., and Bischofberger, N. (1990) Synthesis, hybridization properties and antiviral activity of lipid-oligodeoxynucleotide conjugates. *Nucleic Acids Res. 18*, 3777−3783.
(37) MacKellar, C., Graham, D., Will, D. W., Burgess, S., and Brown, T. (1992) Synthesis and physical properties of anti-HIV antisense oligonucleotides bearing terminal lipophilic groups. *Nucleic Acids Res. 20*, 3411−3417.
(38) de Smidt, P. C., Le Doan, T., de Falco, S., and van Berkel, T. J. C. (1991) Association of antisense oligonucleotides with lipoproteins prolongs the plasma half-life and midifies the tissue distribution. *Nucleic Acids Res. 19*, 4695−4700.
(39) Zalipsky, S., Puntambekar, B., Boulikas, P., Engbers, C. M., and Woodle, M. C. (1995) Peptide attachment to extremities of liposomal surface grafted PEG chains: preparation of the long-circulating form of laminin pentapeptide, YIGSR. *Bioconjugate Chem. 6*, 705−708.
(40) DeFrees, S. A., Phillips, L., Guo, L., and Zalipsky, S. (1996) Sialyl Lewis x liposomes as a multivalent ligand and inhibitor of E-selectin mediated cellular adhesion. *J. Am. Chem. Soc. 118*, 6101−6104.
(41) Allen, T. M., Brandeis, E., Hansen, C. B., Kao, G. Y., and Zalipsky, S. (1995) A new strategy for attachment to sterically stabilized liposomes resulting in efficient targeting to cancer cells. *Biochim. Biophys. Acta 1237*, 99−108.
(42) Kirpotin, D., Park, J. W., Hong, K., Zalipsky, S., Li, W.-L., Carter, P., Benz, C. C., and Papahadjopoulos, D. (1997) Sterically stabilized anti-HER2 immunoliposomes: design and targeting to human breast cancer cells in vitro. *Biochemistry 36*, 66−75.
(43) Spragg, D. D., Alford, D. R., Greferath, R., Larsen, C. E., Lee, K.-D., Gurtner, G. C., Cybulsky, M. I., Tosi, P. F., Nicolau, C., and Gimbrone, M. A. (1997) Immunotargeting of liposomes to activated vascular endothelial cells: a strategy for site-selective delivery in the cardiovascular system. *Proc. Natl. Acad. Sci. U.S.A. 94*, 8795−8800.

BC980002X